KUOPION YLIOPISTON JULKAISUJA C. LUONNONTIETEET JA YMPÄRISTÖTIETEET 211
KUOPIO UNIVERSITY PUBLICATIONS C. NATURAL AND ENVIRONMENTAL SCIENCES 211

HEIKKI NIEMINEN

Acoustic Properties of Articular Cartilage

Effect of Composition, Structure and Mechanical Loading

Doctoral dissertation

To be presented by permission of the Faculty of Natural and Environmental Sciences
of the University of Kuopio for public examination in Auditorium ML3,
Medistudia building, University of Kuopio,
on Friday 11th May 2007, at 12 noon

Department of Physics, University of Kuopio
Institute of Biomedicine, Anatomy, University of Kuopio
Department of Clinical Physiology and Nuclear Medicine
Kuopio University Hospital and
University of Kuopio

KUOPION YLIOPISTO

KUOPIO 2007

Distributor: Kuopio University Library
P.O. Box 1627
FI-70211 KUOPIO
FINLAND
Tel. +358 17 163 430
Fax +358 17 163 410
http://www.uku.fi/kirjasto/julkaisutoiminta/julkmyyn.html

Series Editors: Professor Pertti Pasanen, Ph.D.
Department of Environmental Sciences

Professor Jari Kaipio, Ph.D.
Department of Physics

Author's address: Department of Physics
University of Kuopio
P.O. Box 1627
FI-70211 KUOPIO
FINLAND
Tel. +358 50 338 9932
Fax +358 17 162 585
E-mail: heikki.nieminen@uku.fi

Supervisors: Professor Jukka Jurvelin, Ph.D.
Department of Physics
University of Kuopio

Docent Juha Töyräs, Ph.D.
Department of Clinical Neurophysiology
Kuopio University Hospital

Reviewers: Dr. Bahaa Seedhom, Ph.D.
Division of Bioengineering
Academic Unit of Musculoskeletal Diseases
Leeds Medical School
Leeds University, UK

Assistant Professor Elisa Konofagou, Ph.D.
Department of Biomechanical Engineering
Columbia University, New York, USA

Opponent: Associate Professor Yongping Zheng, Ph.D.
Department of Health Technology and Informatics
Hong Kong Polytechnic University, Hong Kong

ISBN 978-951-27-0689-1
ISBN 978-951-27-0784-3 (PDF)
ISSN 1235-0486

Kopijyvä
Kuopio 2007
Finland

Nieminen, Heikki. Acoustic Properties of Articular Cartilage: Effect of Composition, Structure and Mechanical Loading. Kuopio University Publications C. Natural and Environmental Sciences 211. 2007. 80 p.
ISBN 978-951-27-0689-1
ISBN 978-951-27-0784-3 (PDF)
ISSN 1235-0486

ABSTRACT

Articular cartilage is connective tissue that provides low friction surfaces where bones come into contact and, during locomotion and standing it distributes the loads applied to the joint, minimizing the stresses on the subchondral bone. Osteoarthrosis (OA) is a severe joint disease characterized by collagen disruption, proteoglycan depletion and impaired mechanical properties. In OA, the joint cartilage is exposed to increased wear and this can lead to damaging bone-to-bone contact. The degenerative process causes pain to the patient and, finally, dysfunction of the diseased joint. Diagnosis of OA at the initial stage is essential in order to slow down the degenerative process. Unfortunately, the current clinical techniques are incapable of diagnosing early OA. Earlier studies have suggested that ultrasound may be used to detect OA changes in cartilage structure and composition. Further, mechanical indentation has been combined with ultrasound measurements to enable determination of cartilage thickness and compressive strains, and in this way it is possible to obtain a more accurate determination of the mechanical properties of cartilage. However, it is not known whether the possible compression-related changes in acoustic parameters affect mechano-acoustically determined mechanical properties.

This study attempts to clarify the effects of structure and composition of articular cartilage and mechanical loading on acoustic properties of the tissue. Acoustic properties of normal and enzymatically or spontaneously degenerated bovine articular cartilage were studied. Acoustic parameters, *i.e.* ultrasound reflection at cartilage surface, speed and attenuation, were related to tissue structure, composition and mechanical properties, as assessed by reference histological, biochemical and mechanical measurements. Ultrasound speed and attenuation in human, bovine and porcine cartilage was also studied under mechanical loading. Errors introduced into the mechano-acoustically determined mechanical properties through compression-related variation in ultrasound speed were evaluated. A novel model describing compression-related variations of ultrasound speed in human patellar cartilage was established by relating ultrasound speed with compression-related variations in collagen orientation and composition. For reference, a sample-specific finite element (FE) model was constructed by implementing realistic orientation and composition of cartilage as revealed by histological analyses, Fourier transform infrared imaging and water content analyses.

The ultrasound reflection coefficient at the cartilage surface was found to be sensitive at detecting degradation of superficial collagen. The ultrasound speed and attenuation were significantly related to composition, structure and degeneration of cartilage. Ultrasound speed and attenuation were also affected by the mechanical stress and deformation to which cartilage was subjected. The variation in ultrasound speed, although minor, was found to introduce errors into mechano-acoustically measured strain and elastic modulus. The model constructed in this thesis predicted compression-related variation of ultrasound speed with good accuracy, suggesting that variations in collagen orientation and water content in cartilage can determine changes in ultrasound speed during compression.

The results indicate that acoustic properties are related to the structure and composition of articular cartilage. Ultrasound measurements, when accurately measured *in vivo*, could be of benefit in the diagnostics of early OA. However, mechano-acoustic measurements of the mechanical properties of articular cartilage along the axis of ultrasound propagation may be subject to significant errors due to compression-related variation in the ultrasound speed. Further studies are needed to reveal whether compression-related errors in mechano-acoustic measurements of articular cartilage can be avoided.

Universal Decimal Classification: 534-8, 534.321.9, 534.7, 620.179.16, 620.179.17
National Library of Medicine Classification: WE 300, WE 348, WE 103, QT 34, WN 208
Medical Subject Headings: Cartilage, Articular/physiology; Cartilage, Articular/anatomy & histology; Osteoarthritis/diagnosis; Proteoglycans; Collagen; Acoustics; Ultrasonics; Ultrasonography; Mechanics; Biomechanics; Stress, Mechanical; Elasticity; Materials Testing; Finite Element Analysis

To my parents, Marja-Leena and Risto

ACKNOWLEDGMENTS

This study was carried out during the years 2000-2007 in the Department of Physics and Institute of Biomedicine, Anatomy, University of Kuopio, and in the Department of Clinical Physiology and Nuclear Medicine, Kuopio University Hospital and University of Kuopio.

There are numerous people without whom completing this project would have been impossible.

I wish to express my deepest gratitude to my primary supervisor, Professor Jukka S. Jurvelin, Ph.D., for his unselfish and devoted supervision throughout the years. I wish to thank him also for his support and understanding especially during the difficult times. Working in his research group, Biophysics of Bone and Cartilage (BBC), has been a great honor.

I am indebted to my secondary supervisor, Docent Juha Töyräs, Ph.D., for his catching enthusiasm and the never-ending ideas that have kept my work freshly germinating. His dedicated and humorous attitude has always been exemplary and highly inspiring.

I give my cordial thanks to the official pre-examiners, Dr. Bahaa Seedhom, Ph.D. and Assistant Professor Elisa Konofagou, Ph.D., for their constructive critique to improve my thesis. I am grateful to Ewen MacDonald, D.Pharm., for the linguistic review.

It has been inspirational to work within a colourful research environment with highly intelligent colleagues. My special thanks go to my "room-mate", Mikko Nissi, M.Sc., whos joyful and positive attitude and constructive discussions have made working in the research group more than a pleasure. I am grateful to Professor Heikki Helminen, M.D., Ph.D., for providing various resources and the warm and fartherly support throughout the project. I wish to thank Jani Hirvonen, M.Sc. (Eng.), and Matti Timonen, B.Sc., for their momentous contribution to software programming. I am highly grateful to Petro Julkunen, M.Sc. (Eng.), for his effort in the modeling of articular cartilage mechanics. I wish to thank Jarno Rieppo, M.D., for his essential contribution in the microscopy techniques. I am thankful for Mikko Lammi, Ph.D., and Kari Törrönen, M.Sc., for their invaluable help with biochemical analyses. I am grateful to Mrs. Eija Rahunen and Mr. Kari Kotikumpu for the skillful preparation of histological samples. I wish to thank Docent Ilkka Kiviranta, M.D., Ph.D., and Atria Lihakunta Oyj (Kuopio, Finland) for providing material for the study. I am thankful to Simo Saarakkala, Ph.D., for the rewarding "ultrasonic" discussions throughout this project. I wish to express my earnest thanks to the following, current and emeritus members, of the BBC-group: Mikko Hakulinen, Ph.D., Antti Kallioniemi, M.Sc. (Eng.), Erna Kaleva, M.Sc., Janne Karjalainen, M.Sc. (Eng.), Panu Kiviranta, B.M., Rami Korhonen, Ph.D., Jatta Kurkijärvi, M.Sc., Mikko S. Laasanen, Ph.D., Eveliina Lammentausta, M.Sc., Pauno Lötjönen, physics student, Juho Marjanen, M.Sc., Ossi Riekkinen, M.Sc. and Tuomo Silvast, M.Sc. I wish to thank the Biomedical Ultrasound Group, University of Kuopio, for seamless collaboration. I am highly grateful to Dr. Derrick White, Ph.D., for his constructive criticism towards my work.

I am highly grateful for financial support from the Technology Development Center (TEKES), Helsinki, Finland (project 40714/01); Kuopio University Hospital, Kuopio,

Finland (EVO, projects 5103 and 5173); Academy of Finland, Helsinki, Finland (projects 205886 and 47471); The Graduate School for Musculoskeletal Diseases, Finland and European Union (BMH4-CT97 to 2437); The Finnish Cultural Foundation of Northern Savo, Kuopio, Finland; The Finnish Cultural Foundation, Helsinki, Finland; Finnish Academy of Science and Letters, Helsinki, Finland; Foundation for Advanced Technology of Eastern Finland, Kuopio, Finland; and The Foundation of Aleksanteri Mikkonen, Kuopio, Finland.

I wish to thank the numerous friends for sharing and support at all stages of the project. Especially, I want to thank Petteri Hirvonen, Jukka Hynynen and Teemu Ruohonen for helping to refresh my thoughts by replacing numbers by melodies.

There are measures that are incalculable. The support and love of my dear parents, Marja-Leena and Risto Nieminen, have been invaluable throughout my life and make me eternally grateful to them. Their belief in me and encouragement have been indispensable and essential during this project, but most importantly, during the difficult times. I wish to express my warmest hug to my lovable and loving sister, Anni Nieminen, for being the sparkling delight and for always being there for me. I wish to thank my dear brother, Miika Nieminen, and his family, for their joyous smiles, tickle-laughs and love, and Miika for "leading the way" into cartilage research. I owe my deepest gratitude to God for showing me what is important in life, for giving me the strength and for creating such a phenomenal tissue, articular cartilage, which has kept me busy during the past years.

Kuopio, 22th April 2007

Heikki Nieminen

LIST OF ABBREVIATIONS AND NOTATIONS

D	deep region of cartilage
ePLM	enhanced polarized light microscopy
GAG	glycosaminoglycan
FE	finite element
FFT	fast Fourier transform
FC	femoral condyle
FG	femoral groove
FLC	femoral lateral condyle
FMC	femoral medial condyle
FTIRI	Fourier transform infrared imaging
LM	light microscopy
LPG	lateral patellar groove
M	middle region of cartilage
OA	osteoarthrosis
PA	parallel to articular surface
PAT	lateral upper quadrant of patella
PBS	phosphate-buffered saline
PE	perpendicular to articular surface
PG	proteoglycan
PGF	patellar groove of femur
PLM	polarized light microscopy
PP	proximal phalanx
PSF	patellar surface of femur
Rad.	radial region of cartilage
RF	radio-frequency
S	superficial region of cartilage
Tang.	tangential region of cartilage
TLP	tibial lateral plateau
TMP	tibial medial plateau
TP	tibial plateau
Trans.	transitional region of cartilage

a	indenter diameter
A	amplitude
AIB	apparent integrated backscatter
$A(f)$	amplitude spectrum
BUA	broadband ultrasound attenuation
c	ultrasound speed
c_{ISCM}	ultrasound speed determined using *in situ* calibration method
c_p	specific heat at constant pressure
c_v	specific heat at constant volume
$C_{\mathrm{H_2O}}$	water content

CQI	cartilage quality index
d	diameter
d_i	distance from the transducer to saline-cartilage interface at location i
e	void ratio, *i.e.* fluid volume to solid volume ratio
E	elastic modulus, *i.e.* Young's modulus
E_{dyn}	elastic modulus under dynamic compression, *i.e.* dynamic modulus
E_{eq}	elastic modulus at mechanical equilibrium
f	frequency
f_p	peak frequency
$G(f)$	power spectrum
IRC	integrated reflection coefficient
j	imaginary unit
k	wave number
K_a	adiabatic bulk modulus
K_i	isothermal bulk modulus
h	sample thickness
n	number of samples
$nBUA$	normalized broadband ultrasound attenuation
p	statistical significance
P	load
r	Pearson correlation coefficient
r_S	Spearman's correlation coefficient
r_{xy}	cross-correlation coefficient
R	reflection coefficient
R_{sm}	reflection coefficient at the sample-metallic plate interface
R_{st}	reflection coefficient at the sample-transducer interface
SD	standard deviation
S_{Mankin}	Mankin score
$S_{E_{\text{dyn}}}$	sub-score corresponding to E_{dyn}
$S_{E_{\text{eq}}}$	sub-score corresponding to E_{eq}
SEM	standard error of mean
$S_{\text{H}_2\text{O}}$	sub-score corresponding to $C_{\text{H}_2\text{O}}$
S_{hist}	sub-score corresponding to S_{Mankin}
t	time
T	transmission coefficient
TOF	time-of-flight
u	particle displacement amplitude
URI	ultrasound roughness index
x	distance
Z	acoustical impedance
α	attenuation coefficient
α_{amp}	amplitude attenuation coefficient
α_{abs}	absorption coefficient
α_{int}	integrated attenuation coefficient
α_{sc}	scattering coefficient

β	mean collagen orientation
δc	measurement error in ultrasound speed
δE	error in mechano-acoustically determined elastic modulus
δh	measurement error in sample thickness
$\delta \varepsilon$	error in mechano-acoustically determined strain
δTOF	measurement error in time-of-flight
Δc	change in ultrasound speed
Δf	frequency range
Δh	absolute deformation
ΔT	window length
ε	strain
$\varepsilon_{\mathrm{meas}}$	mechano-acoustically measured strain
$\varepsilon_{\mathrm{true}}$	true strain
κ	scale factor
ν	Poisson's ratio
θ	angle of propagation respective to surface normal
ρ	density
ω	angular frequency

LIST OF ORIGINAL PUBLICATIONS

This thesis is based on the following original articles referred to by their Roman numerals:

I Nieminen H.J., Töyräs J., Rieppo J., Nieminen M.T., Hirvonen J., Korhonen R. and Jurvelin J.S., Real-time ultrasound analysis of articular cartilage degradation *in vitro*, *Ultrasound in Medicine and Biology* 28(4):519-525 (2002)

II Nieminen H.J., Saarakkala S., Laasanen M.S., Hirvonen J., Jurvelin J.S. and Töyräs J., Ultrasound attenuation in normal and spontaneously degenerated articular cartilage, *Ultrasound in Medicine and Biology* 30(4):493-500 (2004)

III Nieminen H.J., Töyräs J., Laasanen M.S. and Jurvelin J.S., Acoustic properties of articular cartilage under mechanical stress, *Biorheology* 43(3-4):523-535 (2006)

IV Nieminen H.J., Julkunen P., Töyräs J. and Jurvelin J.S., Ultrasound speed in articular cartilage under mechanical compression, *Ultrasound in Medicine and Biology*, in press, 2007

The thesis contains also previously unpublished data.

Contents

Chapter I

Introduction

Articular cartilage is connective tissue that provides low friction surfaces where bones come into contact and during locomotion and standing it distributes the loads applied to the joint, minimizing the stresses on the subchondral bone [102]. Cartilage exhibits a nonhomogeneous structure and composition [26, 102]. The mechanical anisotropy and fibril reinforced poroviscoelasticity of cartilage provides high adaptivity to varying mechanical stresses and integrity of the tissue essential for full functionality [51]. Cartilage degeneration, osteoarthrosis (OA), is a common musculoskeletal disease with significant socioeconomic consequences [154]. The progressive failure of cartilage leads to denudation of cartilage from bone, which causes pain to the patient and, due to cartilage's limited healing capacity, the outcome is often permanent disability of the diseased joint [25, 27, 40, 75]. This leads to total joint replacement, but these replacements unfortunately have a restricted lifespan [51]. Initial phase of OA is asymptomatic and the earliest signs, which are also regarded as the "point of no return", are softening and fibrillation of the superficial tissue [11, 25, 27, 45]. The diagnosis of the disease at an earlier stage could be beneficial since it might be possible to slow down the degeneration process [25]. However, current clinical techniques are insensitive and have a rather limited capability to differentiate healthy cartilage from tissue with early or progressed OA. Even though traditional X-ray OA diagnostics is noninvasive, it is insensitive at detecting changes in cartilage and, thus, it has been exploited in detecting the joint narrowing typical of advanced progression of OA [25]. Magnetic resonance imaging (MRI), also a noninvasive technique, provides tools for detection of lesions, composition and wear of cartilage [38, 47], but is costly and clinical techniques lack the high resolution needed to reveal microstructural changes. Minimally invasive methods to diagnose OA have also been developed. Arthroscopy is a qualitative and subjective technique enabling only detection of the visual signs of advanced degeneration. Optical coherence tomography (OCT) provides a method to reveal the microstructure of cartilage, but due to its limited penetration it is restricted to the superficial tissue [54]. Electromechanical spectroscopy has been proposed to reveal electrokinetic streaming potentials [16, 44, 129]. However, further developments will still be required to relate the relationships between mechanical stress and streaming potentials with early degeneration of cartilage [51]. Mechanical indentation techniques have been used for the determination of mechanical properties

of cartilage [36, 94, 105]. However, these techniques require thickness information of cartilage, which is not readily available, if one wishes to accurately calculate mechanical properties and therefore the method is prone to gross inaccuracies. Ultrasound imaging and quantitative ultrasound analyses of cartilage have been proposed to potentially reveal OA-like changes within the tissue [104, 130, 145]. However, there are still no clinical applications for ultrasonic cartilage imaging. Ultrasound has been proposed as representing a useful technique for measuring cartilage thickness [1, 63, 98, 103, 125]. Therefore, if it was possible to combine thickness information with mechanical indentation, then the mechanical properties of cartilage could be more accurately measured. Unfortunately, it has been claimed that the ultrasound speed in articular cartilage may vary under mechanical compression [160] and, this may introduce measurement errors in mechano-acoustically measured parameters. However, the true effect of compression-related changes in ultrasound speed on mechano-acoustically measured mechanical properties of articular cartilage has never been quantified.

This thesis aimed at clarifying the relations between the acoustic properties of articular cartilage and cartilage structure and composition. The ultrasound properties of cartilage were investigated in normal and spontaneously or enzymatically degenerated cartilage. Particular attention was paid to how mechanical stress and deformation can affect the ultrasound properties, and mechano-acoustically measured mechanical properties, of cartilage. Thus, this study aimed to establish a model to relate the composition and structure of cartilage under compression with variations in ultrasound speed.

CHAPTER II

Articular cartilage

2.1 Structure and composition

Articular cartilage is avascular and aneural connective tissue located at the ends of bones within the joints [26, 90]. In humans, the thickness of the tissue varies from about 1 mm in the finger joints to over 6 mm in the tibia [12, 39, 51]. Together with the synovial fluid, cartilage permits almost frictionless motion for contacting bones [42, 101]. Cartilage is structurally inhomogeneous, *i.e.* it exhibits a depth-wise variation in structure and composition [26]. The main component of cartilage is the interstitial water with nutrients and ions, representing 60-80 % of the tissue wet weight [25, 26].The mean density of normal articular cartilage is slightly higher than that of water [59]. The solid matrix consists primarily of collagen, proteoglycan (PG) macromolecules and chondrocytes, *i.e.* cartilage cells that synthesize collagen and PG aggregates [25, 26]. Calcified cartilage is located adjacent to bone and is separated from deep cartilage by an interface called the tidemark, which is not present in juvenile tissue [26, 51]. Type II collagen constitutes 90-95 % of the total collagen content, although minor amounts of type IV, IX, X and XI collagen can also be found. Collagen represents about 60 % of the total tissue dry weight [26]. The diameter of collagen fibril varies from 20 to 200 nm [51]. The collagen architecture is organized according to the Benninghoff model [15]. In superficial cartilage, the collagen fibers are densely packed and oriented in parallel to the cartilage surface (Fig 2.1). In the middle region, the collagens are randomly oriented, while in the deep region of cartilage, collagens are oriented perpendicularly to the articular surface. The PG content increases depth-wise towards the deep tissue (Fig 2.1). The core of the PG aggreate is constructed by a hyaluronic acid chain to which the core protein of a glycosaminoglycan (GAG) chain is attached via a link protein [25]. Negatively charged keratan sulfate and chondroitin sulfate molecules attract water, thus, inducing a swelling pressure inside the tissue that is resisted by the collagen network [25]. During prolonged loading of cartilage, water flow occurs within the tissue, and out of the tissue enabling the circulation of nutrients and waste products [140].

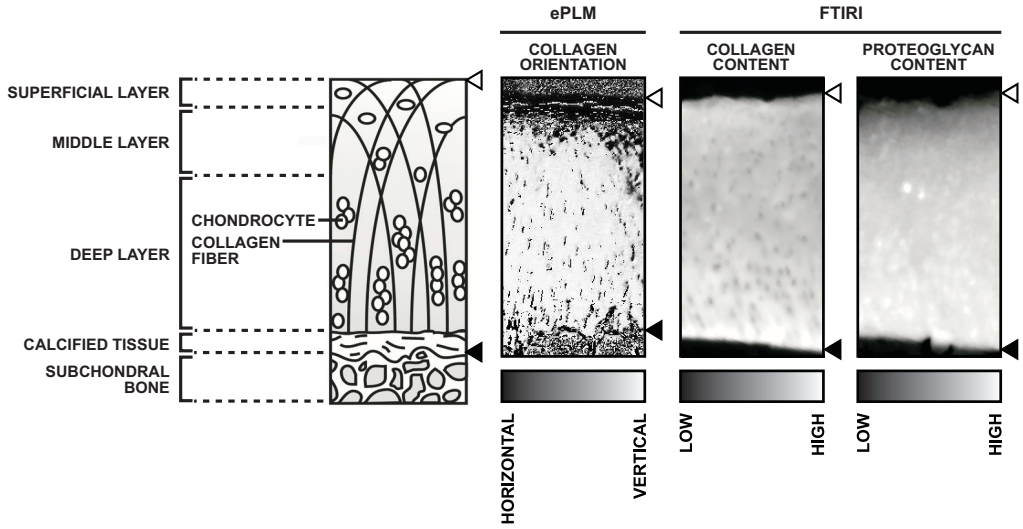

Figure 2.1: Schematic representation of cartilage structure (left). The typical histological image obtained from enhanced polarized light microscopy (ePLM) reveals that collagen is oriented along the surface at the superficial cartilage, whereas in deep layer it is oriented perpendicular to the cartilage surface. Fourier transform infrared imaging (FTIRI) reveals that PG content typically increases from the superficial cartilage towards deep tissue. As a complement of the solid matrix, water content decreases from the superficial to deep cartilage. White and black triangles indicate the cartilage surface and cartilage-bone interface, respectively.

2.2 Mechanical properties

Collagen and PGs are the most important components determining the mechanical integrity of cartilage [23, 26]. Their interactions with the tissue water determine the resilience and compressive stiffness of cartilage [27, 102] as well as establish the anisotropic and poroviscoelastic behaviour of the tissue [62, 95, 102]. The equilibrium modulus of cartilage has been shown to increase along the cartilage depth [82] (Fig. 2.2). The mechanical properties of cartilage vary within a joint [6], from one anatomical location to another [9].

When cartilage is loaded at high rates, it behaves as an incompressible material with no significant fluid flow. The dynamic mechanical properties of cartilage are strongly determined by the integrity of collagen network. Collagen lacks compressive properties, but demonstrates tensile viscoelastic and nonlinear behaviour [60]. Instantaneous stiffness of the tissue is significantly reduced due to the fibrillation of superficial collagen [8]. Under a static load, cartilage settles into a mechanical equilibrium, which is determined primarily by the water-attracting PGs [78]. The high fixed charge density induces the osmotic swelling pressure, defined as the Donnan effect, thus, acting in opposition to the compressive stress [51]. When there is continued stress, then there is a flow of interstitial water, which in turn is controlled by tissue permeability; these changes promote an

intrinsic rearrangement of cartilage matrix [21, 66, 67]. Removal of the very superficial layer of the tissue has been shown to increase water flow and speed up the relaxation process significantly under mechanical loading [140].

The mechanics of cartilage may be described analytically in simplified cases, whereas complex problems require numerical modelling. An analytical elastic single phasic model was first introduced by Hayes *et al.* for indentation of cartilage [53]. Subsequently, single phasic viscoelastic models were used to describe the viscoelastic nature of cartilage by describing cartilage as a combination of linear springs and dashpots [112]. Biphasic models realistically take into account the poroelasticity of the solid matrix, *i.e.* collagen network and PGs and the fluid flow that occurs during prolonged compression [51]. In addition, transversally isotropic biphasic models [34, 152] assume cartilage to be isotropic in the depth-wise planes in parallel to the articular surface. In addition to the biphasic model, the triphasic model [86] considers also the transport of ions through the matrix. Fibril-reinforced poroviscoelastic biphasic models take also into account the collagen architecture. In addition, the newest models consider realistically the collagen microstructure as well as the distributions of fluid, collagen and PGs [60, 149]. Finite element applications of these complex models have been developed to characterize immeasurable properties of articular cartilage.

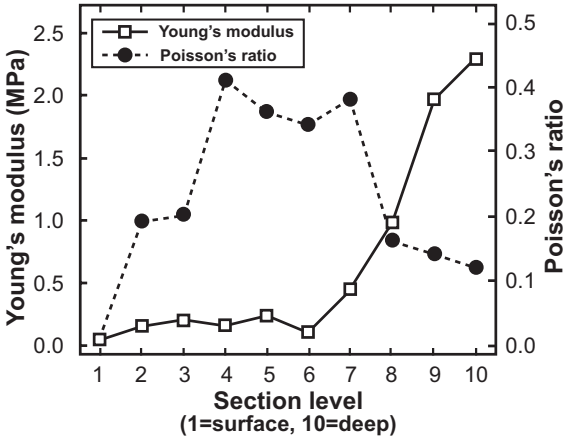

Figure 2.2: Characteristic values of Young's modulus and Poisson's ratio in bovine articular cartilage at different tissue depths. The data has been reproduced from the study by Laasanen *et al.* [82]. While the explanation for the depth-dependence of cartilage Poisson's ratio remains unresolved, it has been proposed that it is related to collagen content, orientation and cross-linking [74, 82].

2.3 Osteoarthrosis

Osteoarthrosis (OA) is a severe musculoskeletal disorder that causes pain and functional disability in patients. Consequently, it has a significant socio-economic impact [124, 131, 154]. Due to the silent nature of OA during its initial stage, the diagnosis of early OA is difficult [25, 32]. The first signs, which are regarded as the "point of no return",

are softening of the tissue due to the fibrillation of collagen network and loss of PGs [11, 27, 45]. These initial signs may be accompanied by small superficial fissures [25]. In advanced OA, the fissures penetrate through cartilage to the subchondral bone and the mechanical integrity of the tissue is impaired due to the disruption of the collagen network. Collagen damage allows swelling of the tissue and loss of PGs [25, 97]. During OA progression, cartilage wear and tear and release of the cartilage fragments to the joint space lead to thinning of the tissue and, consequently, to joint space narrowing. This is followed by increased contact of the bone ends evoking pain. In conjunction with this, the consequent increased deformation of the bone ends leads to dysfunction and immobility of the joint [27, 131]. Adult cartilage possesses poor ability to undergo self-repair, *e.g.* the turnover time of collagen exceeds the human lifespan, although limited repair may occur at lesions penetrating subchondral bone [131]. OA changes have also been shown to associate with stiffening and thickening of subchondral bone as well as with the formation of osteophytes [25, 27, 56, 118]. In advanced OA, cell death may also occur [19, 25]. If cartilage is damaged, the collagen network may not recover, although PG regeneration may occur [40, 75].

CHAPTER III

Acoustic properties of articular cartilage

3.1 Ultrasound basics

Ultrasound is a propagating acoustic vibration with a frequency $>$ 20 kHz. Acoustic waves vibrate and travel longitudinally in gases, liquids and solids. In solids, there are several different types of waves, *e.g.* shear, Rayleigh and Lamb waves, which may also contribute to the wave propagation. Ideally, the simple particle oscillation in longitudinal acoustic vibration may be described with a sinusoidal waveform (Table 3.1, [137]) that satisfies the linear wave equation (Table 3.1, [70, 123, 137]). The wave propagation speed in a homogeneous isotropic material is characterized by its density and mechanical properties (Table 3.1). In conjunction with material density, ultrasound speed defines the acoustic impedance of the material (Table 3.1).

Within an inhomogeneous material ultrasound is subjected to reflections at acoustic interfaces of two materials with different acoustic impedances. If the discontinuities are of the size or smaller than the wavelength of the acoustic wave, the wave is significantly scattered. At a specular reflection, part of the ultrasound energy is reflected according to the reflection coefficient of the acoustic interface (Table 3.1). The transmitted portion of the wave (Table 3.1) is then subjected to refraction according to Snell's law (Table 3.1). Attenuation of ultrasound is not induced only by scattering, but also absorption of energy [146]. In biological tissues, ultrasound energy is typically absorbed via relaxation processes, relative motion, bubble mechanisms or acoustic hysteresis [146, 148]. Attenuation follows the exponential law and the sum of absorption and scattering coefficients give the attenuation coefficient, which in biological materials is highly dependent on the frequency, being either linear or nonlinear depending on the tissue [110, 147] (Table 3.1).

3.2 Acoustic properties of cartilage

Several studies have suggested that the ultrasonic properties of articular cartilage are related to the structural and mechanical properties of the tissue [2, 4, 32, 69, 89, 130, 134, 144, 145, 155]. Ultrasound reflection and scattering have been shown to be sensitive to morphology and the composition of the superficial layer of articular cartilage [3, 32, 33, 115, 128, 145]. The density and ultrasound speed of articular cartilage are slightly higher than those of water [59, 104] exhibiting an acoustic impedance relatively close to that of

Table 3.1: Basic equations in linear wave acoustics.

Parameter	Equation
Simple particle oscillation	$u(x,t) = \mathrm{Re}\left\{u_0 e^{j(\omega t - kx)}\right\} = u_0 \cos\left[\omega\left(t - \frac{x}{c}\right)\right]$
Linear wave equation	$\frac{\partial^2 u}{\partial x^2} = \frac{1}{c^2}\frac{\partial^2 u}{\partial t^2}$
Ultrasound speed in fluid	$c = \sqrt{\frac{K_a}{\rho}} = \sqrt{\frac{\frac{c_p}{c_v}K_i}{\rho}}$
Ultrasound speed in solid	$c = \sqrt{\frac{E(1-\nu)}{(1-2\nu)(1+\nu)\rho}}$
Acoustic impedance	$Z = \rho c$
Reflection coefficient	$R = \frac{A_r}{A_i} = \frac{Z_2\cos\theta_i - Z_1\cos\theta_t}{Z_2\cos\theta_i + Z_1\cos\theta_t}$
Transmission coefficient	$T = \frac{A_t}{A_i} = 1 - R = \frac{2Z_2\cos\theta_i}{Z_2\cos\theta_i + Z_1\cos\theta_t}$
Snell's law	$\frac{\sin\theta_i}{\sin\theta_t} = \frac{c_1}{c_2}$
Attenuation law	$A_1 = A_0 e^{-\alpha x} = A_0 e^{-(\alpha_{\mathrm{abs}} + \alpha_{\mathrm{sc}})x}$
Attenuation in biological tissues	$\alpha(f) = \alpha f^y, 1 \le y \le 2$

A = pressure amplitude
A_0 = initial pressure amplitude
A_1 = pressure amplitude at distance x from the initial location
c = ultrasound speed
c_p = specific heat at constant pressure
c_v = specific heat at constant volume
f = frequency
E = elastic modulus
j = imaginary unit
k = wave number
K_a = adiabatic bulk modulus
K_i = isothermal bulk modulus
t = time
u = particle displacement amplitude
u_0 = maximum particle displacement from rest position
x = distance
α = attenuation coefficient
α_{abs} = absorption coefficient
α_{sc} = scattering coefficient
θ = angle of propagation respective to surface normal
ρ = density
ν = Poisson's ratio
ω = angular frequency
Re{.} = real operator
Subscripts i, r, t refer to incident, reflected and transmitted parameter values.
Indices 1 and 2 refer to the two different materials.

water. Thus, the ultrasound reflection at the articular surface is small at saline-cartilage interface [145]. Superficial fibrillation in human cartilage has been found to induce a wide band of uneven or irregular echoes at superficial and transitional zones, while intact articular surface yields a smooth and a narrow specular-like echo band [104]. Wavelet transform methods have also been applied to study the echo duration at the superficial articular cartilage in an attempt to discriminate osteoarthrotic cartilage from normal cartilage [52, 64]. Integrated reflection coefficient (Table 3.2), determined from B-mode radio-frequency data, has been shown to reveal the superficial cartilage roughness [32, 128] due to the increased scattering [30, 31]. The superficial roughness of cartilage has also been determined using ultrasound roughness index (URI) [85, 128]. Furthermore, ultrasound has been successfully exploited in contouring or imaging of the cartilage surface for detection of lesions [37, 83, 85, 89, 107, 127, 138]. The ultrasound reflection coefficient (Table 3.2) has also been shown to be sensitive to collagen degeneration [145] and to vary at different anatomical locations [84].

Table 3.2: Common ultrasound parameters used to study articular cartilage.

Parameter	Equation
Amplitude attenuation† [145]	$\alpha_{\text{amp}} = \frac{1}{2h} \log_e \left[\frac{R_2 A_1}{R_1 A_2} \left(1 - R_1^2\right) \right]$
Frequency dependent attenuation [134]	$\alpha(f) = \frac{1}{4h} \log_e \frac{G_0(f)}{G_1(f)}$
Integrated attenuation [134]	$\alpha_{\text{int}} = \frac{1}{\Delta f} \int_{\Delta f} \alpha(f) df$
Amplitude reflection coefficient‡ [145]	$R = \frac{A_1}{A_0}$
Frequency dependent reflection coefficient‡ [32]	$R(f) = \frac{A_1(f,z)}{A_0(f,z)}$
Integrated reflection coefficient‡ [32, 33]	$IRC = \frac{1}{\Delta f} \int_{\Delta f} 10 \log_{10} \left\langle \frac{\lvert A_1(f,z)\rvert^2}{\lvert A_0(f,z)\rvert^2} \right\rangle df$
Apparent integrated backscatter‡ [32, 33]	$AIB = \frac{1}{\Delta f} \int_{\Delta f} 10 \log_{10} \left\langle \frac{\lvert A_b(f,z)\rvert^2}{\lvert A_0(f,z)\rvert^2} \right\rangle df$
Broadband ultrasound attenuation [87, 114, 141]	$BUA = \frac{\mathrm{d}}{\mathrm{d}f} \left(10 \log_{10} \frac{A_0(f)}{A_1(f)} \right)$
Normalized broadband ultrasound attenuation [114]	$nBUA = \frac{BUA}{h}$
Ultrasound speed, direct [145]	$c = \frac{2h}{TOF}$
Ultrasound speed, substitution method [113, 114]	$c = c_s \left(1 + \frac{TOF_1 - TOF_2}{TOF_4 - TOF_3} \right)$
Ultrasound speed, *in situ* calibration method [111, 139]	$c_{\text{ISCM}} = \frac{2\Delta h}{\Delta TOF}$
Ultrasound roughness index [128]	$URI = \sqrt{\frac{1}{m} \sum_{i=1}^{m} \left(d_i - \langle d \rangle\right)^2}$

†Indices 1 and 2 refer to values obtained at saline-cartilage and cartilage-bone interfaces, respectively.
‡Indices 0 and 1 refer to values obtained from perfect reflector and sample, respectively.
A = peak-to-peak pressure amplitude
$A(f,z)$ = amplitude spectrum of the pulse reflected at distance z from transducer
$A_b(f,z)$ = amplitude spectrum of the pulse backscattered at distance z from transducer
c_s = ultrasound speed in saline
d_i = distance from the transducer to saline-cartilage interface at location i
f = frequency
$G_0(f)$ = power spectrum of the pulse reflected at distance z from transducer without sample
$G_1(f)$ = power spectrum of the pulse reflected at distance z from transducer with sample
h = cartilage thickness
R = amplitude reflection coefficient
TOF = time-of-flight
TOF_1 = time-of-flight of the pulse reflected from metal plate without the sample
TOF_2 = time-of-flight of the pulse reflected from metal plate with the sample
TOF_3 = time-of-flight of the pulse reflected from saline-cartilage interface
TOF_4 = time-of-flight of the pulse reflected from cartilage-saline interface
Δf = frequency range corresponding to -6 dB level
Δh = absolute deformation
ΔTOF = change in TOF during deformation Δh
$\langle . \rangle$ = spatial average

It has been suggested that the changes in ultrasound attenuation (Table 3.2) could be related to the fibrillar collagen network [115] as well as to PG content [57, 58]. This is supported by the findings in other soft tissues in which ultrasound scattering is related to collagen content [116]. The apparent integrated backscatter (Table 3.2) has been demonstrated to relate to the maturation of rat cartilage [33]. In chemically induced cartilage degeneration, ultrasound attenuation increased [4, 57, 58], but not systematically in all studies [4, 145] (Table 3.3). Although collagen cross-links may play a role [4], increased attenuation may be related to the increase in scattering, as revealed by the stronger echogenicity after chemical degradation [130, 145]. The frequency dependence of ultrasound attenuation has been suggested to increase with collagen content [114]. It has been shown that the slope of frequency dependence of attenuation is steeper in cartilage of an adult rat, 0.41 ± 0.12 dB MHz^{-1} mm^{-1} than the corresponding value in a young rat, 0.25 ± 0.03 dB MHz^{-1} mm^{-1}, at the frequency range 28-70 MHz [114]. The efficient

backscattering and reflection from internal structures has enabled the visualisation of the internal structure of articular cartilage in immature Yorkshire pigs at 50 MHz with an axial resolution of 30 μm [69]. At the same frequency, cartilage defects ranging from 40 to 50 μm could be detected from B-mode images [130]. With respect to the measurement geometries applicable to clinical circumstances, the measurement of absolute attenuation values may be challenging as the reflection coefficient at cartilage-bone is not known. However, the selection of the reflection coefficient at cartilage-bone interface in a realistic range has been found to have negligible effects on the determination of relative changes in attenuation [145].

Table 3.3: Attenuation coefficients (mean $\pm$ SEM or range) measured for articular cartilage.

Species	**Site**	**Type**	**Direction**	***n***	**Attenuation** (dB mm^{-1})	**Frequency** (MHz)	**Study**
human	FC	normal, overall	PE	24	$4.5 - 10.5$	20-40	[57]
		young normal	PE	7	6.2 ± 0.4	30	
		normal	PE	24	7.1 ± 0.4	30	
		papain	PE	24	8.5 ± 0.5	30	
bovine	FC	normal, overall	PE	12	$5.5 - 10.5$	20-40	
		normal	PE	12	6.8 ± 1.2	30	
		interleukin-1α	PE	12	9.1 ± 1.0	30	
bovine	PGF		PE	5	$2.8 - 6.5$† 5.2 ± 1.7†‡	10-40	[134]
bovine	PGF	normal	PA	2	$92 - 147$	100	[4]
			PE		$88 - 105$		
		chondroitinase ABC	PA	2	$40 - 63$		
			PE		$108 - 112$		
		collagen only	PA	2	$77 - 90$		
			PE		$75 - 85$		
		cross-links cleaved	PA	2	$165 - 166$		
			PE		$143 - 185$		

† integrated attenuation
‡ mean $\pm$ SD
FC = femoral condyle
PA = parallel to surface
PE = perpendicular to surface
PGF = patellar groove of femur

According to previous studies, ultrasound speed in articular cartilage is strongly related to the composition and structure of articular cartilage. Ultrasound speed decreases with the reduction of PGs [57, 58, 115, 145] and with the increase in the water content of the tissue [115]. However, another study [104] detected no significant relation between ultrasound speed and water or hydroxyproline and uronic acid contents, which are measures of collagen and PG content, respectively. In contrast, it has been suggested that the ultrasound speed in cartilage increases with the increasing content of collagen [114]. It has been shown that the ultrasound speed in cartilage may be governed by the orientation and cross-links of collagen fibrils [4]. This is supported by the finding that ultrasound speed in collagen was higher along than the corresponding value across the fibril [48, 88]. Previous studies revealed that at 100 MHz and 50 MHz, the ultrasound speed was higher in the deep zone than in the superficial or transitional zones [4, 113]

of bovine cartilage. The ultrasound speed was also significantly higher at all cartilage depths when the ultrasound beam was aligned perpendicular to the articular surface [113]. Pellaumail *et al.* demonstrated a diverse depth-dependence in ultrasound speed for immature rat cartilage, although no significant depth-dependence was revealed for mature cartilage [114]. However, the overall ultrasound speed through the full thickness rat cartilage was higher, 1690 ± 10 m s^{-1} for mature compared to 1640 ± 15 m s^{-1} in the immature rat cartilage (Table 3.4). Previous studies have suggested that ultrasound speed in cartilage varies from one anatomical location to another (Table 3.4).

Ophir and Yadzi [111] introduced a method to determine ultrasound speed in a material under mechanical compression, using the assumption that the ultrasound speed in the material is constant during compression. This method was later used by Suh *et al.* [139] to measure ultrasound speed in articular cartilage with the *in situ* calibration method. However, Zheng *et al.* [158, 160] have suggested that the ultrasound speed in cartilage changes during mechanical compression. This finding may, therefore, introduce errors into the determination of ultrasound speed when the *in situ* calibration method is exploited. However, the magnitude of possible errors in ultrasound speed, *i.e.* those determined using the *in situ* calibration method, has not been investigated.

3.3 Ultrasound and mechano-acoustic measurement techniques

The mechanical integrity of cartilage decreases significantly with the progress of osteoarthrosis [27, 46]. Several mechanical indentation techniques have been developed to detect the tissue stiffness [7, 13, 14, 36, 55, 68, 79, 94, 100, 105, 135]. These methods may provide powerful quantitative techniques for early diagnostics of cartilage degeneration. Indentation techniques often are based on the theory of indentation of single phase elastic materials [53]. The indentation techniques require information on the thickness of the tissue, and if this parameter is unknown, this can lead to measurement inaccuracies in the determination of the elastic modulus, especially with thin cartilage [53].

Ultrasound has been applied for the determination of cartilage thickness [1, 63, 98, 103, 117, 125]. In an attempt to eliminate errors in measured elastic modulus in indentation geometry due to the lacking thickness information, an ultrasound transducer as an indenter has been demonstrated to provide a tool for determination of the tissue thickness [65, 80, 81, 139, 155, 157]. A similar idea has recently been applied to undertake the ultrasound measurement through a water jet that indents the soft tissue [92]. These mechano-acoustic techniques enable, not only determination of mechanical properties of the tissue, but also the acoustic properties that are known to be related to the integrity of articular cartilage [80, 81, 117]. If the indentation method is exploited in the determination of elastic modulus of the material, the ultrasound speed is assumed to remain constant and used to track the compressive displacements. For reliable determination of thickness and, therefore, deformation information, it is important that ultrasound speed in the tissue is accurately known [80, 143].

Acoustic tracking of the internal structures of soft tissue under mechanical stress, *i.e.* ultrasound elastography [17, 18, 28, 77, 108, 109], has enabled the determination of depth-wise elastic properties of articular cartilage [43, 156, 158–160]. However, it is

not known if compression-related changes in ultrasound speed, proposed by Zheng *et al.* [158, 160], affect the determined mechanical properties of articular cartilage in the axis of ultrasound propagation and mechanical compression [158].

Table 3.4: Ultrasound speed in articular cartilage (mean ± SD or range). The measurement direction is demonstrated relative to the cartilage surface. Status indicates the type of sample or the chemical degradation to which the sample had been subjected.

Species	**Site**	**Status**	**Direction**	***n***	**Ultrasound speed** (m s^{-1})	**Frequency** (MHz)	**Study**
bovine	PAT	normal	PE	18	1636 ± 25	50	[113]
			PE (S)	18	1574 ± 29		
			PE (M)	18	1621 ± 34		
			PE (D)	18	1701 ± 36		
			PA (S)	10	1518 ± 17		
			PA (M)	10	1532 ± 26		
			PA (D)	10	1554 ± 42		
bovine	PAT	normal	PE	6	1627 ± 58	10.3	[142]
	FMC	normal	PE	6	1638 ± 18		
	LPG	normal	PE	6	1652 ± 16		
	TMP	normal	PE	6	1602 ± 35		
	talus	normal	PE	6	1721 ± 26		
human	FC	young normal	PE	7	1666 ± 16†	30	[57]
		normal	PE	24	1664 ± 7†		
		papain	PE	24	1642 ± 9†		
bovine	FC	normal	PE	12	1666 ± 8†		
		interleukin-1α	PE	12	1631 ± 17†		
equine	PP	normal, age 5 months	PE	16	1695 ± 160	10	[22]
		normal, age 1.5 years	PE	18	1748 ± 127		
		degenerated, age 3-20 years	PE	42	1675 ± 107		
		overall	PE	76	1696 ± 126		
bovine	PAT	visually normal	PE	24	1654 ± 82	22	[145]
		chondroitinase ABC	PE	12	1646 ± 68		
		collagenase	PE	12	1567 ± 100		
rat	patella	normal, immature	PE	6	1640 ± 15	55	[114]
		normal, mature	PE	6	1690 ± 10		
human	ankle tibia	normal	PE	17	1849 ± 133	20	[153]
	talus	normal	PE	12	1835 ± 67		
	acetabular cup	normal	PE	13	1915 ± 271		
	femoral head	normal	PE	27	1934 ± 191		
	all locations	normal	PE	69	1892 ± 183		
human	FC	visually normal	PE	27	1658 ± 185	25	[104]
		osteoarthritis	PE	40	1581 ± 148		
bovine	FC, PSF, TP	N/A	PE	16	1765 ± 145	N/A	[76]
bovine	PGF	normal	PE (Tang.)	2	$1635 - 1671$	100	[4]
			PE (Trans.)	2	$1617 - 1647$		
			PE (Rad.)	2	$1715 - 1720$		
			PA	2	$1660 - 1690$		
		chondroitinase ABC	PE (Tang.)	2	$1640 - 1670$		
			PE (Trans.)	2	$1631 - 1641$		
			PE (Rad.)	2	$1738 - 1777$		
			PA	2	$1775 - 1793$		
		collagen only	PE (Tang.)	1	1648		
			PE (Trans.)	2	$1620 - 1653$		
			PE (Rad.)	2	$1704 - 1760$		
			PA	2	$1705 - 1744$		
		cross-links cleaved	PE (Tang.)	2	$1650 - 1680$		
			PE (Trans.)	2	$1610 - 1725$		
			PE (Rad.)	2	$1658 - 1716$		
			PA	1	1695		

† mean ± SEM
D = deep region of cartilage
FC = femoral condyle
FMC = femoral medial condyle
M = middle region of cartilage
LPG = lateral patellar groove
PA = parallel to articular surface
PAT = lateral upper quadrant of patella
PE = perpendicular to articular surface
PGF = patellar groove of femur
PSF = patellar surface of femur
PP = proximal phalanx
Rad. = radial region of cartilage
S = superficial region of cartilage
Tang. = tangential region of cartilage
TP = tibial plateu
Trans. = transitional region of cartilage
TMP = tibial medial plateu

CHAPTER IV

Aims of the present study

Ultrasound has been proposed to provide a potential tool for determining the integrity of articular cartilage. However, it is not clear how ultrasound propagation is related to the composition and structure of cartilage. It is also not well known in quantitative terms how the acoustic properties of articular cartilage are affected by mechanical loading and how possible changes in acoustic properties affect mechano-acoustic determination of mechanical properties of articular cartilage.

To clarify these issues, this thesis aimed to

- examine the interdependence of composition of articular cartilage and the acoustic properties of normal and degenerated cartilage
- study the interdependence of structure of articular cartilage and the acoustic properties of normal and degenerated cartilage
- determine the effects of mechanical loading on acoustic properties of articular cartilage
- relate the compression-related changes in ultrasound speed with the structure and composition of articular cartilage
- evaluate the feasibility of using ultrasound techniques for detecting and quantifying cartilage degeneration

CHAPTER V

Materials and methods

This thesis consists of four independent studies. Studies **I** and **II** investigated the effect of composition and structure of articular cartilage on its acoustic properties. The main focus in studies **III** and **IV** was on the effect of mechanical loading on the acoustic properties of articular cartilage. A summary of the materials and methods is presented in Table 5.1.

5.1 Sample preparation

In study **I**, visually normal osteochondral samples (n = 18, d = 9 mm) were prepared from the lateral upper quadrant of 1 to 3 -year-old bovine patellae under sterile conditions (Fig. 5.1). The samples were acoustically measured during enzymatic treatments and being subdivided into three groups according to the treatment: control (n = 6), PG-depleted (n = 6) and collagen-degenerated (n = 6) groups.

For studies **II-IV**, cartilage disks (d = 4 mm) without subchondral bone were prepared under sterile conditions from various anatomical locations (Fig. 5.1). Samples with visually various degenerative stages (**II**) were prepared from the lateral upper quadrant of bovine patella (n = 32). Visually healthy samples (**III**) were prepared from the lateral upper quadrant of human (n = 6), bovine (n = 6) and porcine (n = 6) patellae. Human cartilage samples (**IV**) represented cartilage at various stages of degeneration, as determined visually, and were prepared from different anatomical locations: femoral groove (FG, n = 13), femoral lateral condyle (FLC, n = 13), femoral medial condyle (FMC, n = 13), lateral upper quadrant of patella (PAT, n = 11), tibial lateral plateau (TLP, n = 13) and tibial medial plateau (TMP, n = 13). Bovine samples (**IV**) (n = 6) from lateral upper quadrant of patella were visually normal. The samples were kept moist with Gibco BRL Dulbecco's phosphate-buffered saline (PBS) (Life Technologies, Paisley, Scotland, UK) during all stages of preparation. The samples investigated in studies **II-IV** were stored at -20°C prior to the measurements. Elastomer samples (n = 2, d = 4 mm) and degassed distilled water were used as reference material (**III-IV**). Human patellar samples in study **III** were included in the group PAT (n = 11) for study **IV**.

Table 5.1: Summary of the materials and methods used in this study. All measurements were conducted *in vitro*.

Study	**I**	**II**	**III**	**IV**
Samples	Cartilage with subchondral bone $n = 18$ $d = 9$ mm	Cartilage $n = 32$ $d = 4$ mm	Cartilage $n = 18$ $d = 4$ mm	Cartilage $n = 82$ $d = 4$ mm
Species	Bovine	Bovine	Human, bovine, porcine	Human, bovine
Site	PAT	PAT	PAT	FMC, FLC, FG PAT, TLP, TMP
Degenerative stage	Visually normal and enzymatically degenerated	Visually normal and spontaneously degenerated	Visually normal	Visually normal and spontaneously degenerated
Acoustic measurements	Focused, non-contact, f_p=29.4 MHz	Non-focused, contact, f_p=10.3 MHz	Non-focused, contact, f_p=10.3 MHz	Non-focused, contact, f_p=10.3 MHz and 8.1 MHz
Reference methods	PLM, LM	Mechanical and biochemical measurements, LM, grading by Mankin score and CQI	Mechanical measurements	Mechanical measurements, ePLM, FTIRI, water content, FE modeling

ePLM = enhanced polarized light microscopy
FE = finite element
FG = femoral groove
FLC = femoral lateral condyle
FMC = femoral medial condyle
FTIRI = Fourier transform infrared imaging
LM = light microscopy
PAT = lateral upper quadrant of patella
PLM = polarized light microscopy
TLP = tibial lateral plateau
TMP = tibial medial plateau
d = diameter
f_p = peak frequency
n = number of samples
CQI = cartilage quality index

5.2 Acoustic measurements

In study **I**, the samples were measured at 10-second intervals during the enzymatic digestions using an UltraPAC system (Physical Acoustic Corporation, Princeton, NJ) customized for this individual study. The system was equipped with a focused broadband 29.4 MHz (18.8 to 40.0 MHz, -6 dB) transducer (d = 6.35 mm, radius of curvature = 25.40 mm, model PZ25-0.25"-SU-R1.00", Panametrics, Waltham, MA) (Fig. 5.2A). The transducer was connected to a PAC IPR-100 pulser receiver board (Physical Acoustic Corporation) and *pulse-echo* ultrasound measurements were conducted at 5-minute intervals during the incubation period (6 or 4 hours). The ultrasound signal was digitized at a 500 MHz sampling rate using an 8-bit A/D-board (PAC-AD-500, Physical Acoustic Corporation) and stored for later analysis. The measurement system was controlled using custom software (LabVIEW, version 5.1.1, National Instruments, Austin, TX) designed specifically for study **I**.

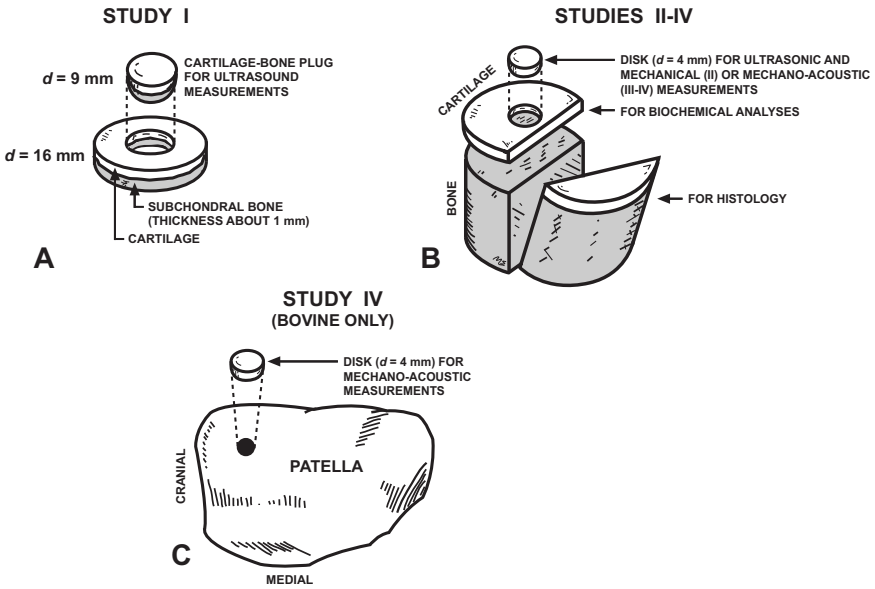

Figure 5.1: Sample preparation. **A.** In study **I**, osteochondral plugs (d = 16 mm) from the lateral upper quadrant of bovine patella were extracted using a drill with a hollow bit and an autopsy saw. The bone was trimmed with a diamond saw, leaving about 1 mm of subchondral bone beneath the cartilage. The final osteochondral samples (d = 9 mm) were subsequently prepared with a steel punch. **B.** In studies **II-IV**, osteochondral plugs (d = 16 or 19 mm) from various anatomical locations were extracted using a drill with a hollow bit and an autopsy saw. Subsequently, cartilage disks were detatched from the bone and adjacent cartilage using a razor blade and a biopsy punch. Adjacent tissue was subjected to biochemical analyses and histology. **C.** In study **IV**, the bovine cartilage disks were extracted from the lateral upper quadrant of patella using a razor blade and a biopsy punch.

Special immersion fluids were used (**I**) for degradation of PGs or collagen. Control samples were incubated during the acoustic measurements without enzyme for 6 hours at 37°C, 5% CO_2 atmosphere in Gibco BRL MEM (Life Technologies) supplemented with 70 μg ml^{-1} L-ascorbic acid (Sigma Chemical Co., St. Louis, MO), 100 μg ml^{-1} streptomycin (Sigma), 100 U ml^{-1} penicillin (PAA Laboratories, Linz, Austria), 200 mM L-glutamine (PAA Laboratories) and 2 μg ml^{-1} fungicide (Gibco BRL Fungizone, Life Technologies). For enzymatic treatments, a similar solution was used, however, supplemented with 30 U ml^{-1} of collagenase type VII (C 0773, Sigma) or 200 μg ml^{-1} of trypsin (T 0646, Sigma). Trypsin enzyme was used to digest primarily PGs (digestion period: 4 hours), although trypsin has also been reported to degrade minor amounts of collagen [50]. Collagenase was used to degrade type II collagen (digestion period: 6 hours) [136]. The enzymatic digestions were conducted to induce degradation of superficial collagen or depletion of PGs, typical signs of early OA [27]. Prior to the ultrasound measurements, the sample and specific treatment solution were warmed up separately in an incubator

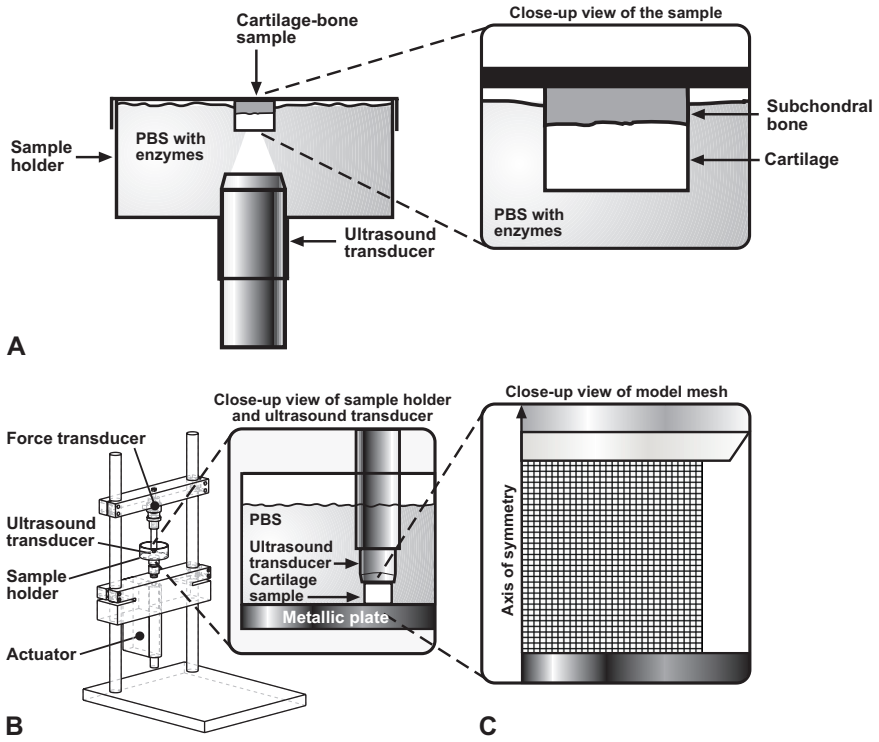

Figure 5.2: A. Ultrasound measurement geometry used in study **I**. **B.** Mechano-acoustic material testing device used in studies **II-IV**. **C.** Schematic representation of the 1050 4-node element FE mesh used in the modeling of collagen orientation and the void ratio during compression of articular cartilage.

at 37°C (5 % CO_2 atmosphere). This was followed by the ultrasound measurement simultaneously with enzymatic degradation. After the ultrasound measurements, the sample was rinsed in PBS and, to terminate the enzymatic action, immersed in PBS with enzyme inhibitors: 5 mM ethylene diamide tetraacetic acid (EDTA, Riedel-de-Haen, Seelze, Germany), 5 mM benzamidine HCl (Sigma Chemical Co., St. Louis, MO) and 5 μg l^{-1} phenylmethylsulfonyl fluoride (Sigma Chemical Co.).

All samples in studies **II** and **III** and human samples in study **IV** were immersed in PBS supplemented with enzyme inhibitors, 5 mM EDTA (Riedel-de-Haen) and 5 mM benzamidine HCl (Sigma Chemical Co.) during the acoustic and mechanical testing to protect the sample from proteolytic degradation. A special measurement solution, instead of PBS, was used due to the long duration of the protocol (about 17 hours, (**IV**)): Dulbecco's modified Eagle's medium (low glucose with L-glutamine) (M0060L, Euroclone, Milano, Italy) supplemented with 15 mM hepes (M0180D, Euroclone), 2 mg ml^{-1} fungizone (Euroclone), 100 μg ml^{-1} streptomycin sulfate (PAA Laboratories) and 100 U ml^{-1} penicillin (PAA Laboratories).

In studies **II-IV**, the samples were measured at room temperature (typically 20°C) using a mechano-acoustic material testing device (Fig. 5.2B), *i.e.* a mechanical testing system [145] empowered by the ultrasound system (UltraPAC, Physical Acoustic Corporation) used in study **I**. The customization of this measurement system has been previously described by Töyräs *et al.* [142]. The sample was positioned between a flat contact transducer (V-116, Panametrics, Waltham, MA) (transducer tip dia. = 5.4 mm, element dia. = 3.2 mm, peak frequency: 10.3 MHz, 7.1-14.2 MHz, -3 dB [142]) and a polished metallic plate (Fig. 5.2B). Different transducer (M-116, Panametrics) was used for bovine samples (transducer tip dia. = 5.4 mm, element dia. = 3.2 mm, peak frequency: 8.1 MHz, 4.6-14.6 MHz, -6 dB) (**IV**). After placing the sample between the metallic plate and the ultrasound transducer, the first contact of the transducer with cartilage surface was monitored using a load cell (model 31, Honeywell Sensotec, Columbus, OH) attached to the ultrasound transducer. The axial positioning and mechanical compression of the sample was conducted using a high-precision actuator (PM1A, Newport, Irvine, CA) (bidirectional repeatibility: 0.1 μm, accuracy of incremental motion: 0.05 μm). In study **II**, the samples were first acoustically tested and then subjected to mechanical measurements. In studies **III-IV**, the samples were simultaneously subjected to acoustic measurement and mechanical loading. Acoustic measurements in study **II** were conducted at 10 % pre-strain to ensure a uniform contact at the transducer-cartilage and cartilage-metal plate interfaces. This was followed by mechanical testing of the tissue. The compressive conditions, during which the acoustic measurements were conducted in studies **III** and **IV**, are described in Section 5.3.1.

5.3 Reference methods

Various reference methods were applied to relate composition, structure and mechanical loading with the acoustic properties of articular cartilage.

5.3.1 Mechanical testing

Mechanical properties of articular cartilage were characterized in unconfined compression geometry (Fig. 5.2B) (**II-IV**). In study **II**, articular cartilage was mechanically tested after acoustic measurements using a stress-relaxation protocol (pre-strain: 10 %, ramp velocity: 2 mm s^{-1}, strain: 10 %, relaxation time: 2400 s). This was followed by 3 cycles of sinusoidal loading at 1 Hz with 1 % strain amplitude. For the samples in study **III** and human cartilage samples in study **IV**, 3 steps of subsequent 5 % stress-relaxation tests were conducted (pre-strain: 5 %, ramp velocity: 1 μm s^{-1}, relaxation criteria: 39 Pa min^{-1}). The final stress-relaxation step of the measurement was followed by 3 cycles of sinusoidal loading at 1 Hz with 1 % strain amplitude. In study **IV**, bovine cartilage samples were used to test whether ultrasound speed in cartilage was dependent on the applied strain-rate. A 10 % pre-strain was used for bovine samples to ensure full contact. Following this stage, a 5 % strain step was applied (relaxation time: 1000 s) and, subsequently, the strain was restored to the original pre-strain value (10 %, strain: 5 %, relaxation time: 3600 s). This test cycle was repeated 11 times using different strain rates (Table 5.2). The order of applied strain rates was randomised

separately for each sample to avoid the possible effect of test order and the long duration of the measurement protocol (about 17 hours) on the observations. Two identical control measurements (strain rate: 5.0 % s^{-1}) were conducted for the sample before and after the entire measurement protocol (Table 5.2) to ensure that the measurement protocol did not affect the ultrasound properties of the sample.

Table 5.2: The strain rates used for the mechano-acoustic stress-relaxation testing of bovine cartilage samples (pre-strain: 10 %, strain: 5 %, relaxation time: 1000 s) (**IV**). After each stress-relaxation test, the strain was restored to the original pre-strain value, 10 % (relaxation time: 3600 s) before the subsequent stress-relaxation test. The order of tests 1-11 was randomised individually for each sample. Ultrasonic measurements were conducted at the beginning and at the end of each ramp compression.

Type of stress-relaxation test	**Strain rate (% s^{-1})**	**Duration of compression (s)**
Control	5.0	1
Test 1	17	0.3
Test 2	10	0.5
Test 3	5.0	1
Test 4	2.5	2
Test 5	1.0	5
Test 6	0.50	10
Test 7	0.17	30
Test 8	0.083	60
Test 9	0.025	200
Test 10	0.010	500
Test 11	0.0050	1000
Control	5.0	1

After the ultrasound measurements (**I**), cartilage thickness was measured at the location of the ultrasound measurements using the needle-probe technique [63]. A sharp needle was pushed through the cartilage at a constant speed using the actuator. The force by which the tissue resists penetration was recorded as a function of the penetration distance with a load cell (model 31, Honeywell Sensotec) attached to the needle. The distance between the cartilage surface and the cartilage-bone-interface, *i.e.* tissue thickness, was determined from the variations of the resistant force.

In studies **II-IV**, cartilage thickness was determined from the actuator as the distance between the transducer and the metallic plate.

In studies **II** and **III**, the elastic modulus at mechanical equilibrium, E_{eq} was derived as a stress-to-strain ratio (Fig. 5.3A), whereas dynamic modulus, E_{dyn}, *i.e.* elastic modulus under dynamic loading, was determined as the ratio of stress and strain amplitudes at 1 Hz.

5.3.2 Histological and biochemical analyses

Polarized light microscopy (PLM) [10, 71, 99] was applied (**I**) to study the organisation of collagen network in normal and degenerated cartilage. Enhanced polarized light microscopy, ePLM, [35, 119] was exploited to reveal the depth-wise collagen orientation in

human articular cartilage (**IV**). In studies **I** and **II**, the PG distribution and content in articular cartilage was examined under light microscopy (LM) from safranin-O stained histologic sections [72, 73].

To estimate the PG and collagen contents in cartilage, the contents of uronic acid ($n = 32$) and hydroxyproline ($n = 28$), respectively, were analyzed biochemically (**II**) [20, 132]. Fourier transform infrared microscopy imaging (FTIRI) was used to determine the relative spatial and depth-wise distribution of collagen and PGs [120] (**IV**). The water content, $C_{\mathrm{H_2O}}$, in cartilage was determined as follows (**II**, **IV**): After immersion of the sample in PBS, extra water was removed from the sample and the wet weight of the sample was determined (high precision balance Mettler AE 240, Mettler Toledo AG, Greifensee, Switzerland). The sample was freeze-dried and the dry weight of the sample was measured. The water content was defined by dividing the difference between wet weight and dry weight by the wet weight. By exploiting FTIRI data and information on total water content, the spatial mass fractions of water, collagen and PGs were calculated for four randomly selected human patellar cartilage samples (**IV**) by utilizing the following assumptions: complement of water is solid matrix, of which 2/3 is collagen and 1/3 is PGs [120].

To provide information on the structural integrity of cartilage (**II**), cartilage samples were histologically graded as follows. Histologic sections, subjected to safranin-O staining, were ″blind-coded″ and observed under LM by three individual investigators according to the Mankin score [96]. The sample-specific Mankin score, S_{Mankin}, was calculated as the mean of the three scores determined by these three investigators and rounded to the closest integer. In this study, S_{Mankin} ranged from 0 to 10. The samples were then divided into three degenerative groups by S_{Mankin}: intact ($n = 11$, $S_{\mathrm{Mankin}} = 0$), moderate degeneration ($n = 11$, $S_{\mathrm{Mankin}} = 1$ to 3) and advanced degeneration groups ($n = 10$, $S_{\mathrm{Mankin}} = 4$ to 10) [106].

A novel cartilage quality index, CQI, was established (**II**) to provide more objective information on the integrity of cartilage among samples [106]. This was achieved by considering simultaneously several parameters related to degenerative stage of cartilage, *i.e.* E_{eq}, E_{dyn}, $C_{\mathrm{H_2O}}$ and S_{Mankin}. For each of these parent parameters, sub-scores from 0 to 10, *i.e.* $S_{E_{\mathrm{eq}}}$, $S_{E_{\mathrm{dyn}}}$, $S_{\mathrm{H_2O}}$ and S_{hist}, were established:

$$S_{E_{\mathrm{eq}}} = \begin{cases} \left[10(1-\frac{E_{\mathrm{eq}}}{0.55\mathrm{MPa}})\right]_{\mathrm{int}} & ,0 \le E_{\mathrm{eq}} \le 0.55\mathrm{MPa} \\ 0 & ,E_{\mathrm{eq}} > 0.55\mathrm{MPa} \end{cases} \tag{5.1}$$

$$S_{E_{\mathrm{dyn}}} = \begin{cases} \left[10(1-\frac{E_{\mathrm{dyn}}}{12\mathrm{MPa}})\right]_{\mathrm{int}} & ,0 \le E_{\mathrm{dyn}} \le 12\mathrm{MPa} \\ 0 & ,E_{\mathrm{dyn}} > 12\mathrm{MPa} \end{cases} \tag{5.2}$$

$$S_{\mathrm{H_20}} = \begin{cases} 0 & ,C_{\mathrm{H_20}} < 75\% \\ \left[\frac{10\left(C_{\mathrm{H_20}}-75\%\right)}{15\%}\right]_{\mathrm{int}} & ,75 \le C_{\mathrm{H_20}} \le 90\% \\ 10 & ,C_{\mathrm{H_20}} > 90\% \end{cases} \tag{5.3}$$

$$S_{\mathrm{hist}} = \begin{cases} S_{\mathrm{Mankin}} & ,0 \le S_{\mathrm{Mankin}} \le 10 \\ 10 & ,S_{\mathrm{Mankin}} > 10 \end{cases}, \tag{5.4}$$

where operation $[\cdot]_{\text{int}}$ stands for rounding of the value to the closest integer. Sub-score 0 stands for the parent parameter value that is typical for healthy cartilage. Correspondingly, 10 stands for the value typical of cartilage with advanced degeneration. Finally, the sub-scores were added up to form CQI:

$$CQI = S_{E_{\text{eq}}} + S_{E_{\text{dyn}}} + S_{\text{H}_2\text{O}} + S_{\text{hist}}. \tag{5.5}$$

CQI, thus, gives integer values from 0 to 40 representing an estimate of the overall cartilage quality, *i.e.* 0 and 40 standing for perfectly healthy and severely degenerated cartilage, respectively. It is important to note that this scoring system may apply only to young bovine patellar cartilage investigated with identical methods as used in study **II**.

5.4 Ultrasound analyses

Ultrasound analyses were conducted using a radio-frequency (RF) signal recorded and digitally stored during the acoustic or mechano-acoustic measurements. The ultrasound reflection coefficient at the saline-cartilage interface (**I**) was defined as

$$R_1(t) = \frac{A_1(t)}{A_0}, \tag{5.6}$$

where $A_1(t)$ is the peak-to-peak amplitude of the echo received from the cartilage surface. A_0 is the peak-to-peak amplitude recorded from a perfect reflector, *i.e.* saline-air interface, measured at the same distance from the transducer as was the case for cartilage. The M-mode visualisation for trypsin-digested samples (**I**) was created by plotting the envelope of A-mode RF signal, calculated as the absolute value of the fast Hilbert transform, as a function of incubation time.

The ultrasound speed in all studies was determined as a function of measurement time, t, as follows:

$$c(t) = \frac{2h(t)}{TOF(t)}, \tag{5.7}$$

where $h(t)$ is the cartilage thickness and TOF time-of-flight of the ultrasound pulse back-and-forth in the tissue as a function of measurement time, t. Since no swelling of the tissue was detected from the ultrasound pulse-echo signal (**I**), cartilage thickness was assumed to remain constant throughout the measurement protocol. In study **II**, $h(t)$ and $TOF(t)$ and, thus $c(t)$, were only determined in the mechanical equilibrium at 10 % pre-strain. For bovine samples (**IV**), ultrasound speed was determined at the beginning and at the end of the ramp compression. In study **III**, ultrasound speed during the mechanical compression was determined using the *in situ* calibration method [139]

$$c_{\text{ISCM}}(t) = \frac{2\,[h(0) - h(t)]}{TOF(0) - TOF(t)}, \tag{5.8}$$

where $h(0)$ is the cartilage thickness before pre-strain and $h(t)$ is the cartilage thickness during the stress-relaxation protocol as a function of time, t. $TOF(t)$ was determined as

the time difference between the echoes reflecting from cartilage-saline and cartilage-bone interfaces (**I**). In the time-domain, each acoustic interface was located at the zero-crossing point that preceded the first echo amplitude rising over the background noise level. In studies **II-IV**, $TOF(t)$ was the time difference between the two ultrasound echoes arising from the cartilage-metallic plate interface after the pulse had travelled back-and-forth in the sample $m+\frac{1}{2}$ and $m+\frac{3}{2}$ times ($m = 1$ or 2) (Fig. 5.3B). Cross-correlation method [29] has been successfully used to determine TOF through full-thickness cartilage or in tracking of ultrasound echo displacements inside articular cartilage under mechanical compression [156]. Thus, $TOF(t)$ was determined using the cross-correlation function [29]:

$$r_{xy}(k) = \frac{\frac{1}{J-1}\sum_{j=1}^{J}(x(j)-\bar{x})(y(j+k)-\bar{y})}{\sqrt{\frac{1}{J-1}\sum_{j=1}^{J}(x(j)-\bar{x})^2 \frac{1}{J-1}\sum_{j=1}^{J}(y(j)-\bar{y})^2}}, \tag{5.9}$$

where $r_{xy}(k)$ is the correlation coefficient and x and y represent the two different A-mode RF signal vectors containing either only the first or the second ultrasound echo, respectively. In each vector, the elements outside the echo of interest were set to zero. Variables j or k are the sample indices of vectors x and y or cross-correlation function r_{xy}, respectively. J is the length of the vectors x and y, and it varied specifically according to sample thickness. TOF was determined as the time lag of the maximum of the cross-correlation function. The ultrasound echoes in vectors x and y were automatically windowed from the original A-mode RF signal vector by positioning the centre of a 300-sample window (duration: 0.6 μs) at the envelope maximum of the echo of interest (Fig. 5.3B). The envelope was calculated as the absolute value of the fast Hilbert transform of the ultrasound pulse-echo signal. The window was chosen to be long enough to capture the entire pulse within the window.

Amplitude attenuation coefficient, α_{amp} (dB mm^{-1}), (**I**) was estimated as [24, 145]

$$\alpha_{\text{amp}}(t) = \frac{4.343}{h(t)} \log_e \left[\frac{R_2 A_1(t)}{R_1(t) A_2(t)} \left(1 - R_1^2(t)\right) \right], \tag{5.10}$$

where $A_1(t)$ and $A_2(t)$ are the peak-to-peak amplitudes of the echoes received from the cartilage-saline and cartilage-bone interfaces, respectively. R_1 is the reflection coefficient defined in equation 5.6 and $R_2 = 0.374$ is the reflection coefficient at the cartilage-bone interface [145, 148]. R_2 was assumed to be the same for all samples.

The amplitude attenuation coefficient (**II-III**), was determined as

$$\alpha_{\text{amp}}(t) = \frac{10}{h(t)} \log_{10} \frac{R_{\text{st}} R_{\text{sm}} A_1(t)}{A_2(t)}, \tag{5.11}$$

where $A_1(t)$ and $A_2(t)$ are the peak-to-peak amplitudes of the echoes received from the cartilage-metallic plate interface after the pulse had travelled through the sample once or three times, respectively, *i.e.* the first and the second echo (Fig. 5.3B). R_{st} and R_{sm} are the ultrasound reflection coefficients at the sample-transducer and sample-metallic plate interfaces, respectively. The site-specific $R_{\text{st}}R_{\text{sm}}$ was determined to be about 0.83 for cartilage (**III**). However in study **II**, $R_{\text{st}}R_{\text{sm}}$ was assumed to be 1.00. The effect of this assumption on results of study **II** has been estimated in Section 5.6.

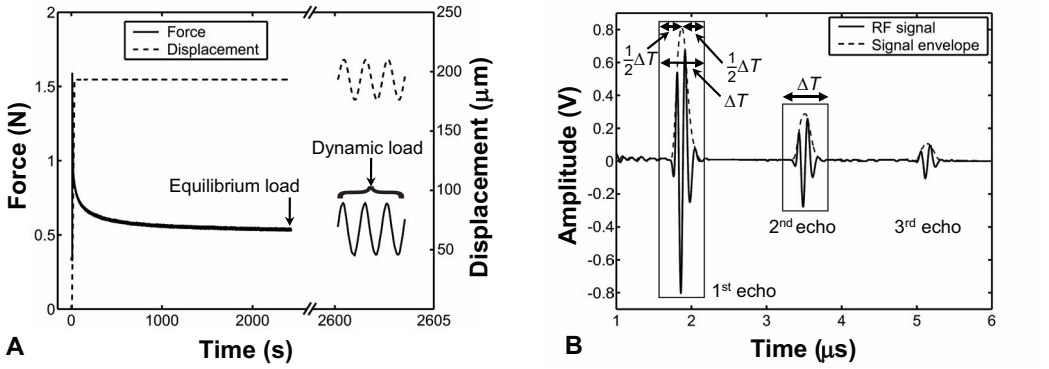

Figure 5.3: **A.** Typical mechanical load and compressive displacement during a stress-relaxation test. **B.** Typical ultrasound pulse-echo signal recorded in the mechano-acoustic measurement geometry. The ultrasound pulse was transmitted at time 0 μs. The centre of windows (ΔT = 0.6 μs), used in the ultrasound analysis, were positioned at the maximum of the signal envelope.

Integrated attenuation coefficient α_{int} (dB mm^{-1}) (**II**-**III**) was determined as [134]

$$\alpha_{\text{int}}(t) = \frac{1}{\Delta f}\int_{\Delta f}\frac{10}{h(t)}\log_{10}\frac{R_{\text{st}}R_{\text{sm}}A_1(f,t)}{A_2(f,t)}df, \tag{5.12}$$

where $A_1(f,t)$ and $A_2(f,t)$ are the amplitude spectra of the echoes received from the cartilage-metallic plate interface after the pulse had travelled back-and-forth in the sample $\frac{1}{2}$ and $\frac{3}{2}$ times, respectively (Fig. 5.3B). Amplitude spectra were calculated as the absolute value of the fast Fourier transform (FFT) of the echoes within the 300-sample window. The vector was zero-padded to 4096 samples prior to FFT calculation. $R_{\text{st}}R_{\text{sm}}$ was determined site specifically and, in study **II**, was assumed to be 1.00. Δf corresponds to the frequency range (5 to 9 MHz), in which logarithm term in equation 5.12 was found to be linear (Fig. 5.4).

Broadband ultrasound attenuation, BUA (dB MHz^{-1}) (**II**), was determined as the slope of the frequency dependence [87, 114, 141]

$$BUA = \frac{\mathrm{d}}{\mathrm{d}f}\left(10\log_{10}\frac{A_1(f)}{A_2(f)}\right). \tag{5.13}$$

From the experimental data, BUA was determined as the slope of the linear fit conducted in the frequency range from 5 to 9 MHz (Fig. 5.4). Normalized broadband ultrasound attenuation, $nBUA$ (dB MHz^{-1} mm^{-1}), was determined by normalizing BUA with the sample thickness, h.

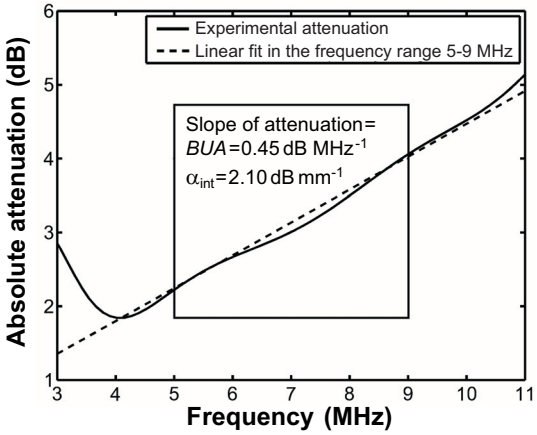

Figure 5.4: Typical ultrasound attenuation in bovine articular cartilage measured with the mechano-acoustic measurement system. Integrated attenuation and BUA were determined within the frequency range of 5-9 MHz.

5.5 Model for ultrasound speed in cartilage during compression

A model to relate compression-related compositional and structural changes with the compression-related variation of ultrasound speed in articular cartilage, was established (Fig. 5.5) (**IV**).

Evenly dense FE meshes were constructed for randomly selected human articular cartilage samples ($n = 4$) in unconfined compression geometry (Fig. 5.2B and 5.2C) according to microscopically acquired geometric information (Section 5.3.2). Each of the sample-specific models consisted of 1050 4-node axisymmetric poroelastic continuum elements, in which the material parameters were implemented using a user-definable subroutine (UMAT) available in ABAQUS 6.4 software (Abaqus Inc., Pawtucket, RI). Initial spatial collagen, PG and water contents and collagen orientation (Section 5.3.2) were implemented with realistic depth-wise distribution into the sample-specific fibril-reinforced poroviscoelastic (FRPVE) model. The implementation of the constitutive laws in the model has been described in earlier publications [150, 151]. From the FE model, relative spatial and depth-wise collagen orientation and the void ratio, *i.e.* fluid volume to solid volume ratio, was solved individually for each sample during the first of the three stress-relaxation steps (**IV**). To determine mean values for orientation and the void ratio under the ultrasound beam, only changes within the ultrasound probe radius (1.5 mm) from the axis of symmetry were solved. Finally, the collagen orientation and void ratio values were averaged over the cartilage depth and ultrasound probe radius.

To explain the detected changes in the values for ultrasound speed during compression, a linear model with collagen orientation and void ratio was fitted to the ultrasound speed, $c(t)$, measured during the first of three stress-relaxation steps for three of the four

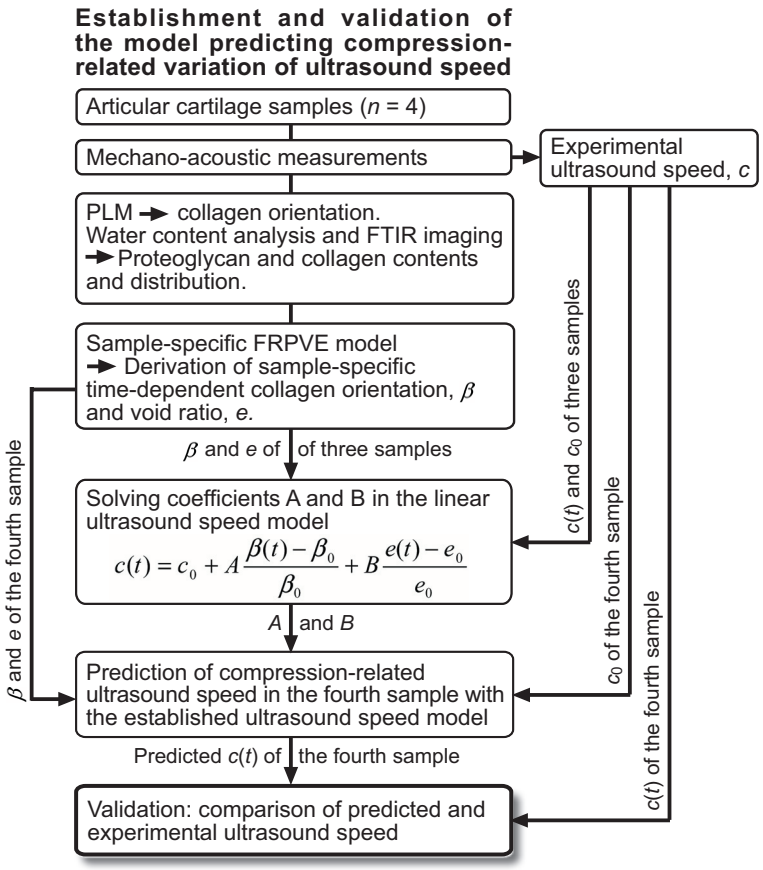

Figure 5.5: A schematic presentation of the establishment and validation of the model predicting variation of ultrasound speed in articular cartilage during mechanical compression.

randomly selected samples:

$$c(t) = c_0 + A\frac{\beta(t) - \beta_0}{\beta_0} + B\frac{e(t) - e_0}{e_0} \tag{5.14}$$

where c_0 is the sample-specific value of ultrasound speed at the beginning of ramp compression, and $\beta(t)$ and $e(t)$ are the mean orientation and mean void ratio, respectively, extracted from FE simulations as a function of stress-relaxation time, t. β_0 and e_0 are the respective initial values.

The mean collagen orientation and the mean void ratio of the fourth randomly selected sample, retrieved from the FE model throughout the stress-relaxation test, and the experimental ultrasound speed data at the beginning of compression, were substituted into the linear ultrasound speed model with the solved constants A and B (equation 5.14). To validate the ultrasound speed model, ultrasound speed, predicted by the model for

the fourth sample, was compared with the experimental ultrasound speed data measured for the same sample.

5.6 Error analyses

The effect of compression-related variation of ultrasound speed in articular cartilage on mechano-acoustically determined mechanical parameters, *i.e.* strain and elastic modulus at ramp compression and at mechanical equilibrium, was evaluated in studies **III** and **IV**. All error simulations were based on indentation geometry, which so far is the only available technique to assess mechanical properties of articular cartilage *in vivo*. The errors were estimated along the axis of compression, which in the present study is the axis of ultrasound propagation. In this geometry, the elastic modulus, E, of cartilage may be expressed as [53]

$$E = \frac{P\,(1-\nu^2)}{2a\kappa\varepsilon h}, \tag{5.15}$$

where P is load, ν the Poisson's ratio, a indenter diameter, κ the scale factor due to the finite and variable tissue thickness, ε the compressive strain and h is the initial sample thickness. If the ultrasound speed, c, is assumed to remain constant along the axis of compression and ultrasound propagation, which is a typical assumption in mechano-acoustic indentation and conventional ultrasound elastography, then errors may be introduced into measured strain and elastic moduli provided that c does not remain constant and it is used when determining the compressive deformation. In such a case, the relative errors in the measured strain, $\delta\varepsilon$, and elastic modulus, δE, may be expressed as follows (**III**, **IV**):

$$\delta\varepsilon = \frac{TOF_1(c_1 - c_0)}{c_0 TOF_0 - c_1 TOF_1} \tag{5.16}$$

$$\delta E = \frac{c_0 TOF_0 - c_1 TOF_1}{c_0\,(TOF_0 - TOF_1)} - 1. \tag{5.17}$$

where the index 0 refers to the value in the beginning of ramp compression and index 1 refers to the value at the end of ramp compression or mechanical equilibrium.

The dependence of relative error in strain on the change in ultrasound speed, Δc, and ultrasound speed, c_0, may be derived (**IV**) as follows:

$$\delta\varepsilon = \left(1 - \frac{c_0}{c_0 + \Delta c}\right)\left(\frac{1}{\varepsilon_{\text{true}}} - 1\right) \tag{5.18}$$

The simulation was conducted under 5 % strain. Thus, $\varepsilon_{\text{true}} = 0.05$, Δc varied from 0 to the maximum change discovered experimentally for bovine samples (**IV**) and the ultrasound speed was assumed to be 1630 m s$^{-1}\pm$ 10 % [142]. The measured strain, with the compression-related error involved, can be expressed as (**IV**)

$$\varepsilon_{\text{meas}} = 1 - \frac{c_0}{c_0 + \Delta c}\,(1 - \varepsilon_{\text{true}})\,. \tag{5.19}$$

Thus, the error in the measured elastic modulus depends on Δc and c_0 as follows:

$$\delta E = \varepsilon_{\text{true}} \left[1 - \frac{c_0}{c_0 + \Delta c} \left(1 - \varepsilon_{\text{true}} \right) \right]^{-1} - 1 \tag{5.20}$$

The simulation was conducted under similar conditions as for equation 5.18.

The technical limitations for the determination of the ultrasound speed variations were derived by exploiting the law for propagation of uncertainty. The measurement error in ultrasound speed, δc, attributable to the limitations of the measurement system, may expressed as

$$\delta c = \left[\left(\frac{2}{TOF} \right)^2 (\delta h)^2 + \left(\frac{2h}{TOF^2} \right)^2 (\delta TOF)^2 \right]^{\frac{1}{2}}, \tag{5.21}$$

where $\delta TOF = 1$ ns and $\delta h = 0.05$ μm are the measurement accuracies for time-of-flight and thickness, respectively. c and h represent ultrasound speed and thickness variation ranges in the samples (**II**-**IV**).

In the determination of attenuation (**II**), it was assumed that $R_{\text{st}} R_{\text{sm}} = 1$ in equation 5.11. The attenuation values may be corrected by $R_{\text{st}} R_{\text{sm}} = 0.83$. To evaluate the effect of the assumptions in study **II**, the corrected and uncorrected data sets were compared.

5.7 Statistical analyses

To test statistical variation in ultrasound parameter between two time points non-parametric Wilcoxon signed ranks test was applied. Such analyses were conducted to test the change in ultrasound parameters during enzymatic digestion (**I**) and to test if errors in mechano-acoustically measured strain or elastic moduli were different at the end of ramp compression as compared to their values at mechanical equilibrium (**III**-**IV**). Similarly, Wilcoxon test was used to test whether ultrasound speed at the end of ramp compression was different from that at the beginning in bovine articular cartilage (**IV**). Mann-Whitney U test was used to study (**I**) if ultrasound parameters in digested groups differed from those of control group at the beginning of incubation. Friedman *post hoc* test for n related samples, was applied to test variation of acoustic parameters during stress-relaxation (**III**-**IV**) or their strain-dependence at mechanical equilibrium over the three stress-relaxation steps (**III**). Friedman test for n related samples was applied to study if the decrease in the ultrasound speed in bovine cartilage was dependent on the strain rate (**IV**). Kruskal-Wallis *post hoc* test was applied to test statistical differences in the acoustic parameters between the degenerative groups (**II**) and species (**III**) or change in ultrasound speed from one anatomical location to another (**IV**). Correlations with Mankin score or CQI (r_{S}) were analyzed using Spearman's correlation analysis and correlations (r) between other data sets were tested using Pearson correlation analysis (**II**). Statistical analyses were conducted using SPSS software (version 8.0.1 or 11.5.1, SPSS Inc., Chicago, IL) and a custom-made Matlab program (version 5.3.1 or 6.5.1, Mathworks Inc., Natick, MA).

CHAPTER VI

Results

6.1 Effects of composition and structure on ultrasound properties of articular cartilage

In study **I**, the reflection coefficient (R_1) at the saline-cartilage interface changed substantially from 0.024 ± 0.008 to 0.005 ± 0.002 (-79.2 %, $p < 0.05$, Fig. 6.1A) during the 6-hour collagenase digestion, whereas the respective change during the 4-hour trypsin digestion was smaller, from 0.021 ± 0.008 to 0.019 ± 0.009 (-9.5 %, $p < 0.05$, Fig. 6.1A). Amplitude attenuation (α_{amp}) was found to change from 11.1 ± 1.3 dB mm^{-1} to 11.4 ± 1.3 dB mm^{-1} (+0.3 dB mm^{-1}, $p < 0.05$, Fig. 6.1B) during trypsin digestion, whereas collagenase digestion induced no significant changes in this parameter. The ultrasound speed (c) decreased significantly from 1622 ± 194 m s^{-1} to 1615 ± 195 m s^{-1} (-0.4 %, $p < 0.05$, 6.1C) during trypsin digestion, whereas in the control group, there was a significant increase from 1634 ± 101 m s^{-1} to 1637 ± 101 m s^{-1} (+0.2 %, $p < 0.05$, Fig. 6.1C). However, these changes may not be very substantial. No changes in R_1 or α_{amp} were found in the control group over the incubation period. Cartilage thickness, as measured with the needle-probe technique, was 1950 ± 480 μm in control samples, 1680 ± 230 μm for collagenase-digested samples and 1710 ± 330 μm for trypsin-digested samples. The M-mode visualisation showed that the trypsin penetration front could be distinguished from the ultrasound signal (Fig. 6.2).

In study **II**, integrated attenuation (α_{int}), α_{amp} and c exhibited statistically significant correlations with Mankin score (S_{Mankin}), cartilage quality index (CQI) as well as with the uronic acid and hydroxyproline contents ($p < 0.01$, Table 6.1, Fig. 6.1). The normalized broadband ultrasound attenuation ($nBUA$) correlated weakly, although significantly, with S_{Mankin} and water content ($C_{\text{H}_2\text{O}}$) ($p < 0.05$, Table 6.1). However, no significant associations were established between broadband ultrasound attenuation (BUA) and the reference parameters. Values of α_{int} and α_{amp} in the advanced degeneration group differed significantly ($p < 0.01$, Table 6.2) from those of intact cartilage. α_{amp} distinguished also cartilage with moderate degeneration from intact cartilage ($p < 0.05$, Table 6.2).

Qualitatively, apparent proteoglycan (PG) loss was observed in Safranin-O -stained sections under light microscopy after trypsin digestion (**I**) and in cartilage with moderate

or spontaneous degeneration (**II**). No PG depletion was found in collagenase-digested (**I**), control (**I**) or intact cartilage (**II**). In study **I**, some minor collagen degeneration was observed under polarized light microscopy (PLM) in the superficial cartilage of the collagenase-digested group, whereas in the trypsin or control groups, no changes were found.

Table 6.1: Pearson correlation coefficients between the measured parameters ($n = 28 - 32$) (**II**). Correlation coefficients against Mankin score (S_{Mankin}) and cartilage quality index (CQI) were calculated using the Spearman's correlation analysis. High correlations were established between the ultrasound speed (c) and the reference parameters.

	α_{int}	α_{amp}	$nBUA$	BUA	c
α_{amp}	0.989†	-	-	-	-
$nBUA$	0.805†	0.767†	-	-	-
BUA	0.428‡	0.345	-	-	-
c	0.784†	0.796†	0.381†	0.004	-
S_{Mankin}	-0.567*†	-0.571*†	-0.367*‡	-0.061*	-0.755*†
CQI	-0.655*†	-0.658*†	-0.329*	0.128*	-0.872*†
E_{eq}	0.470†	0.480†	0.058	-0.157	0.790†
E_{dyn}	0.620†	0.641†	0.185	-0.166	0.898†
$C_{\text{H}_2\text{O}}$	-0.647†	-0.684†	-0.350‡	0.019	-0.799†
Uronic acid	0.653†	0.683†	0.273	-0.086	0.879†
Hydroxyproline	0.639†	0.659†	0.224	-0.154	0.863†

† corresponds to statistical significance $p < 0.01$
‡ corresponds to statistical significance $p < 0.05$
* calculated using Spearman's correlation analysis
α_{amp} = amplitude attenuation
α_{int} = integrated attenuation
BUA = broadband ultrasound attenuation
c = ultrasound speed
$C_{\text{H}_2\text{O}}$ = water content
CQI = cartilage quality index
E_{dyn} = dynamic modulus
E_{eq} = elastic modulus at mechanical equilibrium
$nBUA$ = normalized broadband ultrasound attenuation
S_{Mankin} = Mankin score
Hydroxyproline = hydroxyproline content
Uronic acid = uronic acid content

6.2 Effects of mechanical loading on ultrasound properties of articular cartilage

The values of c or ultrasound speed determined using the *in situ* calibration method (c_{ISCM}) did not vary significantly across the species at the mechanical equilibrium of the pre-strain step ($p > 0.05$, Fig. 6.3) (**III**). However, there were significant differences ($p < 0.01$) in α_{amp} and α_{int} between bovine and porcine samples (Fig. 6.3).

In bovine samples (**III**), α_{amp} and α_{int} changed during the mechanical ramp compression ($p < 0.05$), whereas no statistically significant changes were discovered in human or porcine cartilage (Fig. 6.3). During the mechanical relaxation, attenuation values returned towards the original value at the equilibrium of pre-strain (Fig. 6.3). c and

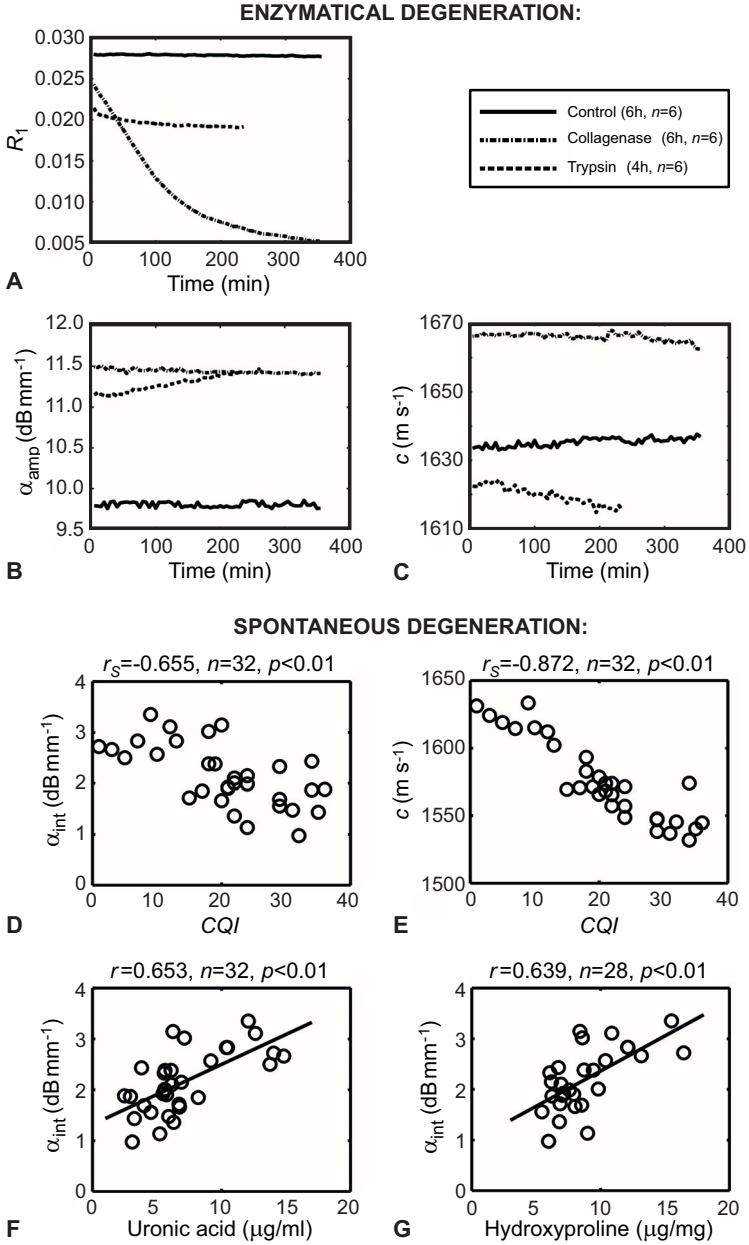

Figure 6.1: Reflection coefficient at the saline-cartilage interface (**A**) at 29.4 MHz (**I**). Ultrasound speed (c) and attenuation (α_{amp} or α_{int}) as a function of enzymatic digestion (**B-C**) at 29.4 MHz (**I**) and as a function of the structural and compositional properties of cartilage (**D-G**) at 10.3 MHz (**II**). The reflection coefficient at superficial cartilage was significantly related to the degenerative stage of collagen network. The ultrasound speed was strongly related to the spontaneous degeneration of cartilage.

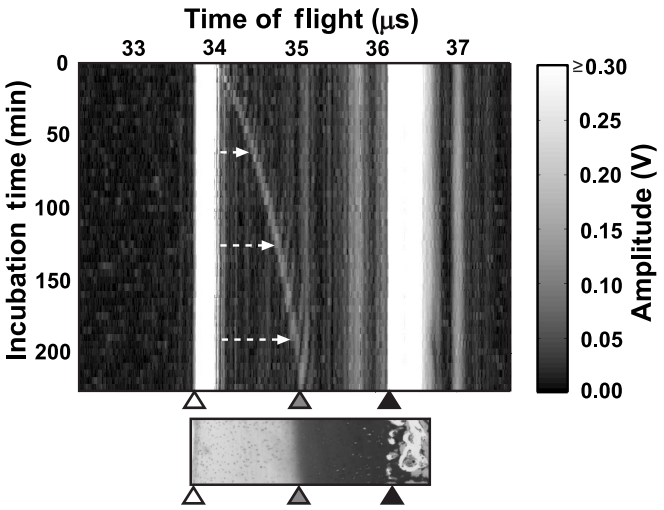

Figure 6.2: M-mode visualisation (top) of articular cartilage during trypsin digestion and a histologic section of the safranin-O stained sample (below) after trypsin digestion (**I**). The superficial cartilage and cartilage-bone interface are indicated with hollow and black triangles, respectively. The trypsin penetration front (arrows, grey-filled triangle) could be tracked from the ultrasound signal.

c_{ISCM} varied significantly in human ($p < 0.01$ and $p < 0.05$, respectively) and bovine ($p < 0.05$) cartilage during ramp compression and mechanical relaxation. However, no significant changes in c or c_{ISCM} were observed for porcine cartilage. c, α_{amp} and α_{int}, at the beginning of ramp compression, showed no statistically significant strain-dependence over the 3 stress-relaxation steps ($p > 0.05$). The reference measurements with degassed distilled water displayed no changes in c, α_{amp} or α_{int} during the measurement protocol similar to that used for cartilage. Only negligible changes were observed in the measured acoustic properties of elastomer during a stress-relaxation test.

In study **IV**, statistically significant changes ($p < 0.05$) in ultrasound speed were recorded in human articular cartilage at all anatomical locations during the stress-relaxation test (Fig. 6.4A). During the ramp compression, the mean change in ultrasound speed at all locations was -8.9 ± 6.9 m s^{-1} ($p < 0.01$) for human cartilage samples. However, the change of ultrasound speed at all locations, calculated from the beginning of ramp compression to mechanical equilibrium (-1.5 ± 5.5 m s^{-1}), demonstrated no significant changes ($p > 0.05$). The magnitude of the ultrasound speed decrease from ramp beginning to ramp end or mechanical equilibrium was independent of the anatomical location ($p > 0.05$). Variation in ultrasound speed in articular cartilage introduced significant errors into the mechano-acoustically determined strain or the elastic modulus at the end of ramp compression (Table 6.3, **III-IV**). c was not observed to vary in the reference material, *i.e.* elastomer or distilled water (Fig. 6.4A), during the stress-relaxation test.

Table 6.2: Measured acoustic and reference parameters in each degenerative group: intact cartilage ($S_{\text{Mankin}} = 0$), moderate degeneration ($S_{\text{Mankin}} = 1-3$) and advanced degeneration ($S_{\text{Mankin}} = 4-10$) (**II**). Ultrasound attenuation and speed were able to discriminate damaged cartilage from intact cartilage.

	Intact ($n = 10-11$)	Moderate ($n = 10-11$)	Advanced ($n = 8-10$)
α_{int} (dB mm^{-1})	2.65±0.58	2.01±0.45	1.76±0.43†
α_{amp} (dB mm^{-1})	3.12±0.62	2.45±0.48*	2.15±0.51†
$nBUA$ (dB MHz^{-1} mm^{-1})	0.40±0.14	0.27±0.09	0.28±0.08
BUA (dB MHz^{-1})	0.64±0.31	0.46±0.17	0.54±0.17
c (m s^{-1})	1603±27	1572±15	1548±14†
Uronic acid (μg ml^{-1})	10.2±3.5	6.7±1.5	4.1±1.2†**
Hydroxyproline (μg mg^{-1})	10.9±3.4	8.5±1.7	6.7±1.0†
h (μm)	1609±371	1701±265	1945±471†
E_{eq} (MPa)	0.32±0.15	0.26±0.13	0.08±0.08†‡
E_{dyn} (MPa)	7.06±4.83	2.12±1.58	0.54±0.36†‡
$C_{\text{H}_2\text{O}}$ (%)	79.9±2.4	81.6±1.2	84.1±2.6†
CQI	11.6±7.5	19.5±3.6	31.3±3.7

† and ‡ are statistical differences ($p < 0.01$) as compared to intact and moderately degenerated groups, respectively
* and ** are significance of $p < 0.05$ as compared to intact and moderately degenerated groups, respectively. Statistical analyses were not conducted for grouping variables: Mankin score or the parameter in which Mankin score is included (*i.e.*, cartilage quality index, CQI).
α_{amp} = amplitude attenuation
α_{int} = integrated attenuation
BUA = broadband ultrasound attenuation
c = ultrasound speed
$C_{\text{H}_2\text{O}}$ = water content
CQI = cartilage quality index
h = cartilage thickness
E_{dyn} = dynamic modulus
E_{eq} = elastic modulus at mechanical equilibrium
$nBUA$ = normalized broadband ultrasound attenuation
Hydroxyproline = hydroxyproline content
Uronic acid = uronic acid content

By fitting the introduced linear model (equation 5.14, **IV**) simultaneously to the ultrasound speed data of three randomly selected human patellar samples (6.4B), values -160.8 m s^{-1} and -116.4 m s^{-1} were obtained for constants A and B, respectively. Validation of the model was conducted by substituting the time-dependent orientation ($\beta(t)$, $\beta_0 := \beta(0)$) and void ratio ($e(t)$, $e_0 := e(0)$) information and experimentally determined ultrasound speed of a fourth sample at ramp beginning ($c_0 := c(0)$) to equation 5.14, which produced the validation graph (Fig. 6.4B). The error between the prediction by the model and the experimental data at each time point was small, < 0.3 %.

For bovine articular cartilage (**IV**) it was revealed that the ultrasound speed decreased significantly with all strain rates during mechanical compression ($p < 0.05$). The magnitude of the decrease in the ultrasound speed was found to depend on the strain rate ($p < 0.001$, Fig. 6.4C) and remained relatively constant with strain rates ≥ 0.5 % s^{-1}. The simulations show that in instantaneous compression of 5 % strain, the typical change in ultrasound speed, -25 m s^{-1}, induced an error of about -30 % and +40 % to mechano-acoustically measured strain and elastic modulus, respectively (Fig. 6.5). As revealed by

Table 6.3: Estimated error (%, mean ± SD) in the measured strain and elastic modulus of articular cartilage, induced by compression-related variation of ultrasound speed, at the end of ramp compression and at mechanical equilibrium during the first of the three 5 % stress-relaxation steps (**III**-**IV**). The errors introduced into the measured strain and elastic modulus were greater at the end of ramp compression than at mechanical equilibrium ($p < 0.05$).

	Site	n	Error in measured strain (%)		Error in measured modulus (%)	
			Ramp end	Equilibrium	Ramp end	Equilibrium
Human	FG	13	-15.4±13.2	-3.6±12.2	20.9±18.9	5.4±14.5
	FLC	13	-9.8±6.7	-1.3±4.6	11.5±8.5	1.5±4.7
	FMC	13	-13.1±6.5	-2.8±3.5	15.8±9.4	3.0±3.7
	PAT	11	-6.1±9.2†	-1.4±4.5	7.4±9.8	1.6±4.8
	TLP	13	-9.2±4.2	-1.7±4.5	10.3±5.1	1.9±4.8
	TMP	13	-10.0±6.4	-0.9±7.2	11.7±8.0	1.5±8.0
Bovine	PAT	6	-11.8±12.0	-2.5±7.3	15.4±17.9	3.0±7.1
Porcine	PAT	6	-3.2±4.5	0.1±2.6	3.4±4.7	0.0±2.6

† $p = 0.0505$
FG = femoral groove
FLC = femoral lateral condyle
FMC = femoral medial condyle
PAT = lateral upper quadrant of patella
TLP = tibial lateral plateau
TMP = tibial medial plateau

the repeated control measurements at 5 % s^{-1} strain rate for cartilage before and after the actual measurements, ultrasound speed and the change in ultrasound speed during ramp compression did not change ($p > 0.05$) due to the test sequence. Within the test sequence, the mean changes in ultrasound speed during ramp compression for elastomer sample and distilled water, were $+3.5 \pm 0.2$ m $s^{-1}$and -0.1 ± 0.3 m s^{-1}, respectively.

The measurement error that propagated to the ultrasound speed (**II**-**IV**) due to the limitations of the measurement system was estimated to be $< 0.1\%$. For typical cartilage ultrasound speed (1630 m s^{-1} [142]) and thickness in the present study (about 1.7 mm) the estimated error was about 0.05 % or 0.8 m s^{-1}. Thus, the measurement system was sensitive enough to measure changes in the ultrasound speed under compressive conditions. It was revealed that ignoring the reflection coefficients at sample-transducer and sample-metallic plate interfaces (**II**) introduced a systematic error of about +0.45 dB mm^{-1} to the attenuation (Fig. 6.6).

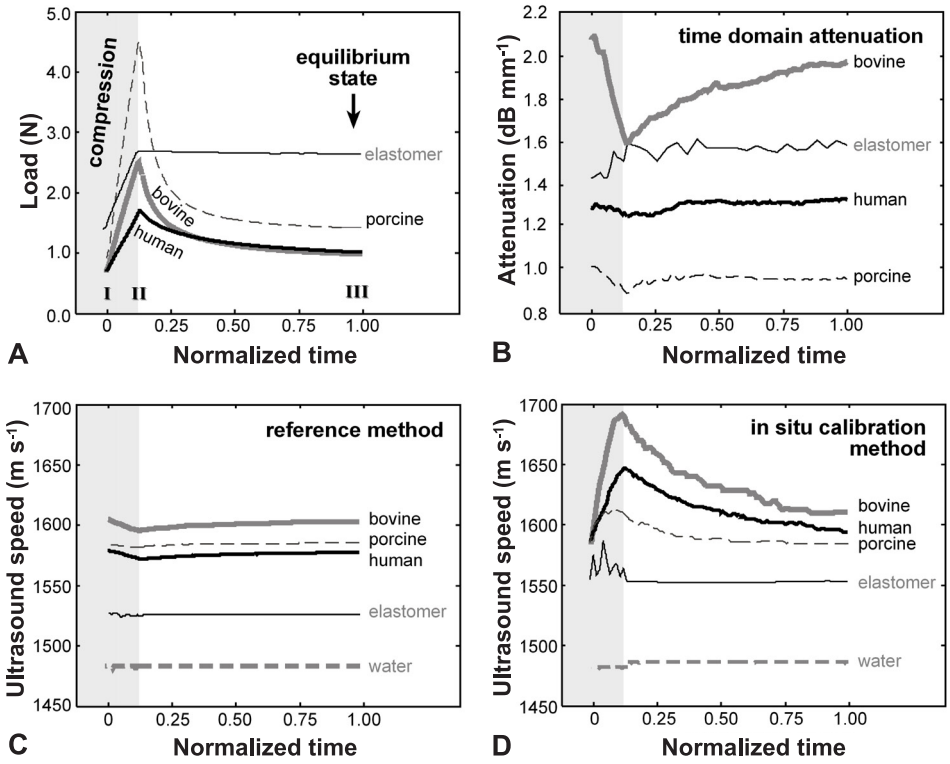

Figure 6.3: Ultrasound parameters under mechanical ramp compression (grey background) and subsequent stress-relaxation (white background) (**III**). Ultrasound speed and attenuation in cartilage were affected by the exposed mechanical loading.

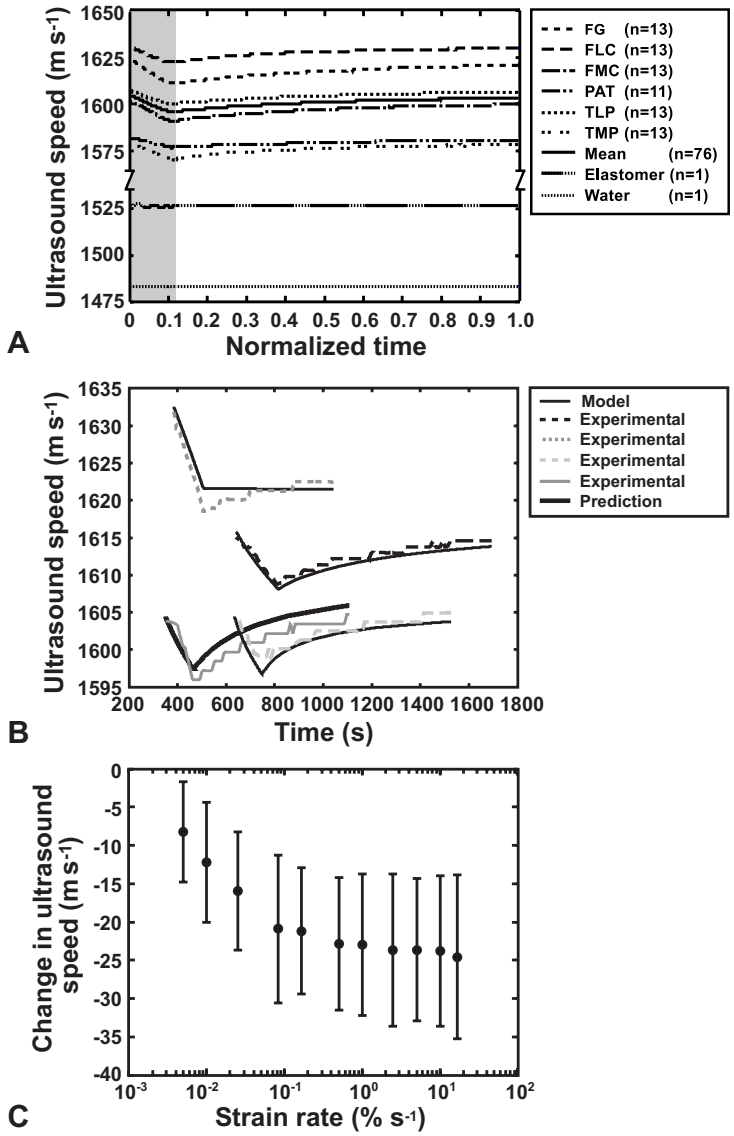

Figure 6.4: A. Ultrasound speed in human articular cartilage extracted from different anatomical locations and in reference materials during a mechanical stress-relaxation test (**IV**). The ramp compression phase is indicated with a grey background. The ultrasound speed was found to vary during mechanical compression in cartilage at all anatomical locations. **B.** Experimentally measured ultrasound speed (dashed line) in three randomly selected human patellar cartilage samples during a stress-relaxation test and the linear ultrasound speed model (equation 5.14) (thin solid black line) fitted to the experimental data (**IV**). Substitution of orientation and void ratio at a given time as well as initial c of a fourth sample into equation 5.14 produced a graph predicting c in the same sample (thick black line). As a validation, the experimental (solid grey line) and predicted c in the fourth sample were compared. The error between the prediction obtained with the model and the experimental data at each time point was small, < 0.3 %. **C.** Change in the ultrasound speed (mean $\pm$ SD, $n = 6$) in bovine cartilage (**IV**) during a 5 % strain ramp as a function strain rate. The errorbars indicate one standard deviation, SD, of mean for 6 samples. The magnitude of the ultrasound speed was found to depend on the strain rate ($p < 0.01$).

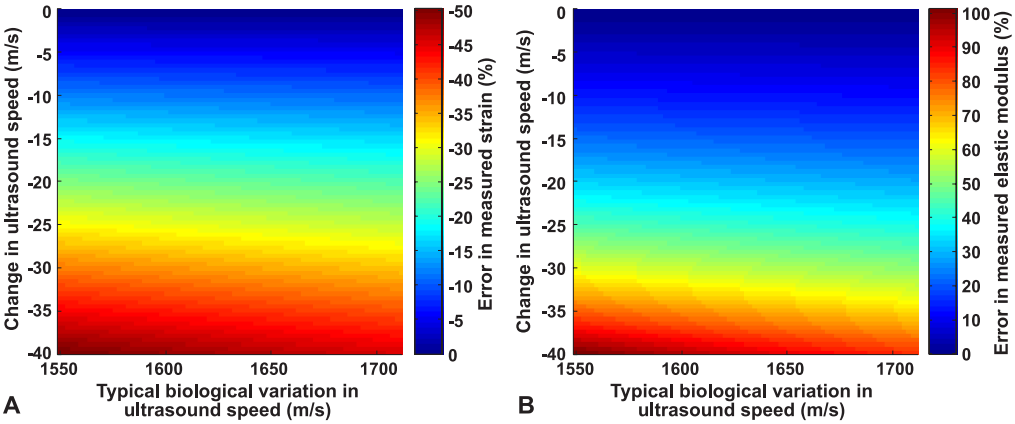

Figure 6.5: Relative error in mechano-acoustically measured strain (**A**) and in elastic modulus (**B**) as a function of the typical variation of ultrasound speed in cartilage and the ultrasound speed change during an instantaneous 5% compression (**IV**). The typical change in the ultrasound speed, -25 m s^{-1}, during instantaneous compression induced an error of -30 % in strain and +40 % in elastic modulus.

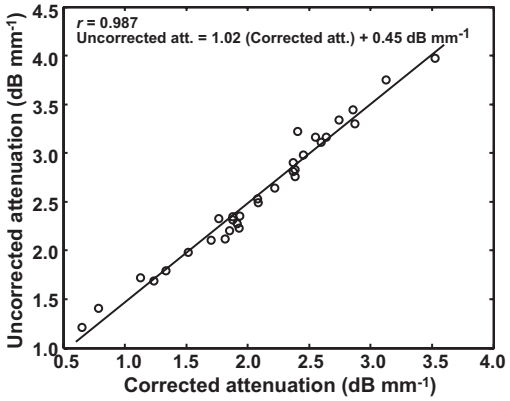

Figure 6.6: Corrected and uncorrected values for amplitude attenuation in mechano-acoustic measurement geometry (**II**). By ignoring the reflection coefficients at the sample-transducer and sample-metallic plate interfaces a systematical error of about +0.45 dB mm^{-1} was introduced into the uncorrected attenuation.

CHAPTER VII

Discussion

This study investigated the acoustic properties of articular cartilage and their dependence on the structure, composition and mechanical loading of the tissue. Studies **I** and **II** addressed specifically the relationships of acoustic, structural and compositional properties of cartilage. Studies **III** and **IV** focused on the effect of mechanical loading on the ultrasound and mechano-acoustically determined mechanical parameters of cartilage.

7.1 Effects of composition and structure on ultrasound properties of articular cartilage

According to the existing earlier literature, reflection and scattering of ultrasound at superficial and deeper cartilage layers are related to the tissue structure and composition [32, 104, 145]. Earlier studies have shown that the ultrasound reflection at the articular surface may be more sensitive to the morphology of the superficial tissue than to its collagen content [3, 126, 128]. The present study showed that ultrasound reflection at the cartilage surface was found to be highly sensitive to enzymatic degradation of collagen with the difference in reflection coefficient before and after collagen degeneration being statistically significant (**I**). PLM images revealed reduced collagen integrity suggesting that the decrease in reflection coefficient may be partially related to the increase in scattering at the superficial tissue [128]. As no visual surface fibrillation was observed under LM, the decreased ultrasound reflection coefficient may not, however, be primarily induced by increased scattering. Digestion with collagenase diminishes the collagen content and collagen fibril diameter, possibly increasing water content in the superficial tissue and lowering its density. As a result of collagen cleavage, the ultrasound speed may decrease significantly at the superficial cartilage [49, 155] resulting, together with a lowered tissue density [59], in an acoustic impedance closer to that of the coupling medium, *i.e.* saline. Although not confirmed by Myers *et al.* for articular cartilage [104], protein content has been found to have a significant effect on ultrasound speed in soft tissues [49] and suspensions [155]. Thus, it is likely that enzymatic treatment with collagenase changes the collagen composition and these changes then alter the ultrasound speed of the superficial cartilage. This is supported by the finding that the overall ultrasound speed decreased, although this decrease was not statistically significant, during the col-

lagen degeneration test (-4 m s^{-1}, -0.2 %). Since the effect of collagenase during the 6-hour digestion was confined to the superficial cartilage, the changes in acoustic properties were restricted to only the superficial tissue. This may have only a small effect on the average ultrasound speed through the cartilage thickness, but a more significant effect on the acoustic impedance and, furthermore, a greater impact on the reflection coefficient at cartilage surface.

A small decrease in the reflection coefficient at the superficial cartilage was observed during the trypsin digestion. The decrease in the reflection coefficient may not be explained by the cleavage of PGs, but by the minor collagen degradation [50] that can be induced by trypsin. Since superficial cartilage is poor in PGs, cleavage of PGs may not affect the acoustic impedance of the cartilage surface significantly and, thus, may not determine the reflective properties of cartilage at the cartilage-saline interface to the same extent as changes in collagen. Trypsin induced a higher decrease in ultrasound speed ($p < 0.05$, -7 m s^{-1}, -0.4 %) than collagenase. The effect of trypsin digestion on ultrasound speed may be more impressive due to the effective cleavage of PGs: trypsin digestion occurred at over 50 % of the total cartilage thickness, whereas collagenase digestion was confined only to the superficial tissue. The association of collagen degeneration and ultrasound reflection at the superficial cartilage is in agreement with earlier studies [3, 32, 128, 145], in which ultrasound reflection has been related to the morphological and compositional changes, typical of osteoarthrosis. Thus, measurement of ultrasound reflection coefficient has clear diagnostic potential since it can reveal the integrity of articular surface.

Ultrasound speed was found to strongly relate to the composition of the tissue in osteoarthrotic cartilage (**II**). Relatively high correlations were established between ultrasound speed and the uronic acid, hydroxyproline and water contents. These parameters are related to compositional changes which are characteristic of osteoarthrosis. In osteoarthrotic cartilage, PGs are depleted and the collagen architecture becomes disrupted, which results in tissue swelling [27, 97] and increase in the water content. Any increase in the water content should, according to acoustic mixture laws [5, 41, 133], change the ultrasound speed in cartilage towards that of water, *i.e.* ultrasound speed should decrease. These findings are supported by earlier studies suggesting that ultrasound speed in osteoarthrotic cartilage is lower (1581 ± 148 m s^{-1}) than in normal cartilage (1658 ± 185 m s^{-1}) [104]. However, in that study, the ultrasound speed was not related to the uronic acid or hydroxyproline contents. In the present study, ultrasound speed was found to relate not only to the compositional parameters, but also to structural integrity, *i.e.* Mankin score. However, it is not clear if associations of ultrasound speed against uronic acid, hydroxyproline and water contents reveal a primary relation, as variation in different components are interconnected via cartilage degeneration.

Although ultrasound speed results are consistent in studies **I** and **II**, there are some discrepancies in the attenuation results. In study **I**, attenuation increased with time during the degeneration of PGs, while no significant changes were observed during collagen degradation or control incubation. This is consistent with an earlier investigation [57] where ultrasound attenuation was found to increase after enzymatic degradation of PGs. However in study **I**, attenuation decreased in parallel with the degenerative process.

Several explanations can be suggested for this discordance. First, the structural and compositional changes induced enzymatically may be restricted only to the superficial cartilage and differ significantly from those occurring in spontaneous osteoarthrosis [122]. Digestive enzymes may induce a highly localized acoustic interface that may reflect ultrasound [117, 145, 156] and, thus, block part of ultrasound energy from propagating to the cartilage-bone interface by reflecting or scattering the ultrasound. This explanation is supported by the finding in the M-mode visualisation during trypsin digestion (**I**), in which a new acoustic echo was noted to be induced inside the cartilage. Second, the collagen architecture may be more profoundly damaged in spontaneous osteoarthrosis inducing significant swelling and a more extensive increase in the water content [97] as compared to that achieved during superficial enzymatic treatments. This may result in fewer scatterers per unit length and subsequently result in smaller attenuation coefficients in osteoarthrotic cartilage. It is possible that absorption is affected by both, enzymatic and spontaneous degeneration, thereby inducing changes in attenuation. According to the present results (**II**), attenuation, if it were possible to be measured accurately, could provide clinically useful information on the integrity of cartilage.

The normalized slope of frequency dependency of attenuation, $nBUA$, was found to correlate weakly although significantly ($p < 0.05$) with Mankin score, cartilage quality index and water content (**II**). However, BUA did not associate with any reference parameter. The slope of attenuation may not be a clinically feasible parameter, at least in the frequency range used in the present study, due to its poor capability to differentiate degenerated cartilage from intact tissue.

7.2 Effects of mechanical loading on ultrasound properties of articular cartilage

Ultrasound speed (**III-IV**) and attenuation (**III**) in bovine and human cartilage varied during the mechanical stress-relaxation test. The attenuation values decreased under the ramp compression but became restored to close to the value prior to the ramp compression during mechanical relaxation towards the equilibrium.

The decrease in the ultrasound speed may be explained by the changes in the composition and structure of cartilage. In study **III**, changes in ultrasound speed were suggested to be related to the compression-related variations in the collagen architecture. Ultrasound speed has earlier been found to be higher along than the corresponding speed across collagen fibrils [48, 88]. During mechanical compression, the collagen orientation changes to a more horizontal alignment. Thus ultrasound, in the present measurement geometry (**III-IV**), propagates more effectively across the collagen fibrils than along the fibrils. In study **III**, we proposed that orientational changes affect ultrasound speed not only during ramp compression but also during mechanical equilibration. As revealed by the finite element model (**IV**), variations in collagen orientation may not explain the variation in ultrasound speed during mechanical relaxation, during which changes in collagen orientation were found to be small. However, the water content was found to vary significantly. In study **IV**, we hypothesized that during mechanical relaxation the ultrasound speed is affected not only by orientational changes but even more significantly

by changes in water content. This explanation is supported by the quantitative findings (**IV**) that relate variations in collagen orientation and water content to experimentally determined ultrasound speed. Compression of cartilage induces water flow, which induces a relative increase in the solid matrix content [121]. According to acoustic mixture laws [5, 41, 133], the ultrasound speed should consequently increase. During instantaneous loading, cartilage is incompressible, *i.e.* no significant water flow occurs. Thus, the decrease of ultrasound speed cannot be attributable to changes in the water content. This is in agreement with the explanation suggesting that the collagen orientation controls the variation of ultrasound speed during instantaneous loading. The difference between the predicted variation of ultrasound speed (**IV**) and the experimentally determined ultrasound was small at all time points, < 0.3 %. It should be noted that during mechanical loading of articular cartilage there may be simultaneous changes in several physical phenomena, *e.g.* fluid pressure, solid stress and strain, water flow, temperature variation, and these can all affect the ultrasound speed in cartilage. However, their effect on the measured ultrasound speed may be minor compared to those of collagen orientation and water content. Agemura *et al.* [4] concluded that ultrasound speed may be higher across than along collagen fibers, which is in disagreement with the earlier findings in which the ultrasound speed in the collagen was found to be higher in a direction along the fibril than it was across the fibril [48, 88]. Agemura *et al.* based their explanation on the depth-wise dependence of the ultrasound speed in articular cartilage and suggested that intermolecular cross-linking and depth-wise collagen orientation might control ultrasound speed. However, they did not speculate about the effect of collagen density on their findings, which may account for the differences between the conclusions of the different studies. This is supported by the finding that collagen density may dramatically affect the measured ultrasound speed, as protein content has been found to influence the ultrasound speed in soft tissues [49].

The detected increase in the ultrasound speed during the relaxation phase is in agreement with an earlier study by Zheng *et al.* [160] in which the ultrasound speed in bovine articular cartilage was studied under compression *in situ*. In contrast to the present study, that study [160] revealed ultrasound speed changes to be less than 0.03 % during the mechanical ramp compression, whereas our study (**III**) showed a decrease of about 0.6 % in the ultrasound speed in bovine articular cartilage. The results may differ due to the differences in samples and measurement geometry. In studies **III** and **IV**, samples ($d = 4$ mm) were detached from bone and measurements were conducted under 5 % strain during unconfined compression (*in vitro*). In contrast, in the study by Zheng *et al.* samples ($d = 6.32 \pm 0.08$ mm) were attached to bone and a smaller strain (about 3.4 %) was used in *in situ* geometry, resulting in smaller orientational changes in the collagen architecture.

In the present study, the ultrasound attenuation was affected more sensitively by mechanical loading in bovine articular cartilage than was determined in human or porcine cartilage. The observed change in ultrasound attenuation during ramp compression may be explained by the changes in the cartilage architecture. As the acoustic wave is a moving mechanical disturbance, it is possible that the mechanical and structural anisotropy also produces acoustic anisotropy. Physically, either absorption and/or scat-

tering of ultrasound decreased during ramp compression, especially in bovine cartilage. The re-arrangement of collagen fibers, known to act as significant scatterers of ultrasound [32, 114, 116], may decrease ultrasound scattering and thus reduce the measured attenuation. Although only visually perfect contact at transducer-cartilage and cartilage-metal plate interfaces was accepted, it is not clear if changes in stress can affect scattering, reflection or transmission conditions at these interfaces. However, no trend was found between the peak stresses and the change in attenuation, suggesting that the applied stress does not primarily control compression-related changes of ultrasound attenuation in this measurement geometry.

In study **III**, the *in situ* calibration method (equation 5.8), which assumes that there is a strain-independent ultrasound speed in the measured material, was used to determine the ultrasound speed under mechanical compression. As a reference, a direct ultrasound speed measurement was also applied (equation 5.7). The *in situ* calibration method was found to be prone to systematic errors due to compression-related change of ultrasound speed, especially at the end of ramp compression. However, the measured values at the mechanical equilibrium were closer to the values obtained using the direct ultrasound speed measurement. In clinical applications, ultrasound speed measurement using the *in situ* calibration method may be acceptable if measurements are conducted at mechanical equilibrium. However for practical reasons, ultrasound speed should be measured during instantaneous compression. The use of mechanical equilibrium would be impractical as the mechanical equilibration of the tissue *in vivo* is time-consuming (may take more than one hour [93]) and a rigid *in vivo* measurement system with clamping of the investigated joint would be required for precise measurements. Under practical situations, the *in situ* calibration method may not be accurate enough to differentiate cartilage with advanced degeneration (**II**, ultrasound speed: 1548 ± 14 m s^{-1}) from intact cartilage (**II**, ultrasound speed: 1603 ± 27 m s^{-1}).

The dependence of ultrasound speed on cartilage compression, determined using the *in situ* calibration method, was opposite to that determined using the direct measurement (**III**). This discrepancy is related to the differential nature of the *in situ* calibration measurement and to the assumption that the ultrasound speed remains constant during compression. If the ultrasound speed is not dependent on compression, then the method yields correct speed values. However, if the ultrasound speed changes, then the time-of-flight after compression is affected and the difference in time-of-flight, due to compression, is subjected to uncertainty (equation 5.8). Thus, a decrease in the ultrasound speed results in smaller time-of-flight difference and, consequently, to the observed increase of ultrasound speed, as determined using *in situ* calibration method. As calculation of strain is based on a differential measurement, a similar problem applies to the strain estimation. If the ultrasound speed is not dependent on compression, the strain may be successfully determined by dividing the time-of-flight change due to compression by the time-of-flight through the sample prior to compression (Appendix, **III-IV**). This does not depend on the absolute ultrasound speed within the sample. However, if ultrasound speed changes, *e.g.* decreases, the difference in time-of-flight, due to compression, is unexpectedly small, resulting in underestimated deformation and, therefore, underestimated strain.

Studies **III** and **IV** revealed that mechano-acoustic techniques depend critically on the constancy of the ultrasound speed under mechanical loading. At the end of ramp compression at a low strain rate, the compression-related variation of ultrasound speed in human, bovine or porcine cartilage was found to induce significant errors in the determined strain or elastic modulus where a constant ultrasound speed was assumed. However, the errors were smaller at mechanical equilibrium. Simulations (equations 5.19 and 5.20, **IV**) revealed that a typical decrease in ultrasound speed, -25 m s^{-1}, under instant compression (**IV**) may result in an error of about -30 % and +40 % in mechano-acoustically measured strain and elastic modulus, respectively (Fig. 6.5). In the worst case scenario, the errors in measured strain and elastic modulus can be even higher, about -50 % and +100 %, respectively. This poses a demanding challenge for mechano-acoustic or elastographic measurements of elastic properties along the axis of compression, especially under a high rate compression. As softening of cartilage is related to the early degenerative changes [11, 27, 45], a depth-wise elastographic characterization of tissue strains and elastic modulus could provide clinically invaluable information on the degenerative status of the tissue. However, cartilage exhibits a depth-wise variation in its structure, composition [25, 26] and mechanical competence [61, 80, 91]. The ultrasound speed and attenuation have been shown to vary in a depth-wise manner [4, 113]. Therefore it is possible that compression-related variation of ultrasound speed may behave differently at different depths of cartilage. The applied strain may also depend on the applied strain. Nevertheless, it is possible that these issues do not preclude the clinical use of mechano-acoustic indentation techniques as these methods have been shown to sensitively distinguish between healthy and degenerated tissue [80]. A method to eliminate compression-induced errors in measured elastic properties of articular cartilage needs to be devised.

The reader should recall that the measured ultrasound speed and attenuation parameters in studies **I-IV** are mean values in full thickness cartilage. The results on attenuation and reflection coefficient (**I-III**) may be clearly related to the frequency in use in the measurements. However, the effect of frequency on ultrasound speed may be minor. It should be noted that a variation in the ultrasound speed under mechanical compression may also depend on the measurement protocol, *e.g.* applied strain, and geometry, *i.e.* ultrasound speed may vary differently under *in situ* or *in vivo* (indentation) loading as compared to the *in vitro* (unconfined) geometry used in the present study. The error analysis, using the principle for propagation of uncertainty, revealed that the small error in the measured ultrasound speed (< 0.1 %), due to the technical limitations of the system, does permit acceptable accuracy for determination of the changes in ultrasound speed. In study **II**, the reflection coefficients ($= 1$, *i.e.* perfect reflection) at sample-transducer and sample-metallic plate interfaces may introduce a systematic error into the measured absolute attenuation values. However, this may not affect the interpretation of the results of study **II**. It should be noted that the amount of samples in studies **I-IV** was limited and the measurements were conducted in laboratory circumstances.

Further studies should be conducted to reveal how substantial are the relations between measured acoustic parameters and cartilage structure and composition *in vivo*.

The effect of selected measurement protocol, geometry or ultrasound frequency on these relations also needs attention. As indentation geometry is at present the only *in vivo* feasible geometry which can be used for the determination of cartilage mechanical parameters, it is important to determine whether compression-related changes in ultrasound speed take place *in vivo* and if they significantly affect the mechano-acoustically determined mechanical parameters of articular cartilage.

Chapter VIII

Summary and conclusions

Ultrasound techniques provide unique possibilities to characterize the integrity of articular cartilage and may provide tools for clinical diagnostics of early osteoarthrosis. Mechano-acoustic determination of mechanical properties of cartilage, however, may be affected by compression-related changes in the ultrasound speed during mechanical indentation. The most important findings of this thesis may summarized as follows:

- The reflection coefficient at cartilage surface is strongly related to the integrity of the superficial collagen network. The reflection coefficient may provide a useful parameter for clinical use as the measurement of absolute values of this parameter is technically straightforward.

- Ultrasound speed and attenuation are significantly related to structure, composition and the degenerative stage of the tissue and, therefore, may be clinically feasible for use in the diagnostics of osteoarthrosis. However, *in vivo* measurement of absolute values may be more challenging.

- Broadband ultrasound attenuation or normalized broadband ultrasound attenuation may not suitable for clinical use and the measurement of absolute values is challenging.

- The ultrasound speed in articular cartilage is affected by the mechanical compression of the tissue. The results of the present study suggest that variation in ultrasound speed is controlled by collagen orientation during instantaneous compression and also by the water content and collagen orientation during mechanical relaxation and at equilibrium.

- The ultrasound speed, as determined using the *in situ* calibration method, is at present, the only available method for measuring the ultrasound speed in articular cartilage bonded to underlying bone. However, the method is prone to errors that are induced by the compression-related changes in the ultrasound speed of articular cartilage during mechanical compression.

- The assumption that there is a constant ultrasound speed during mechanical compression may impair the accuracy of the mechano-acoustic measurements of cartilage mechanical properties.

To conclude, the ultrasound properties of articular cartilage are significantly and specifically related to tissue composition and structure as well as to mechanical loading. Ultrasound may hold clinical potential for revealing the changes typically encountered in early osteoarthrosis. However, before arthroscopic ultrasound techniques can be successfully applied in the clinic, several technical challenges will have to be resolved.

1. C. Adam, F. Eckstein, S. Milz, E. Schulte, C. Becker, and R. Putz. The distribution of cartilage thickness in the knee-joints of old-aged individuals-measurement by A-mode ultrasound. *Clin Biomech*, 13(1):1–10, 1998.

2. M. E. Adams and C. J. Wallace. Quantitative imaging of osteoarthritis. *Semin Arthritis Rheum*, 20(6 Suppl 2):26–39, 1991.

3. R. S. Adler, D. K. Dedrick, T. J. Laing, E. H. Chiang, C. R. Meyer, P. H. Bland, and J. M. Rubin. Quantitative assessment of cartilage surface roughness in osteoarthritis using high frequency ultrasound. *Ultrasound Med Biol*, 18(1):51–58, 1992.

4. D. H. Agemura, Jr. O'Brien, W. D., J. E. Olerud, L. E. Chun, and D. E. Eyre. Ultrasonic propagation properties of articular cartilage at 100 MHz. *J Acoust Soc Am*, 87(4):1786–1791, 1990.

5. R. E. Apfel. Prediction of tissue composition from ultrasonic measurements and mixture rules. *J Acoust Soc Am*, 79(1):148–152, 1986.

6. R. C. Appleyard, D. Burkhardt, P. Ghosh, R. Read, M Cake, M. V. Swain, and G. A. Murrell. Topographical analysis of the structural, biochemical and dynamic biomechanical properties of cartilage in an ovine model of osteoarthritis. *Osteoarthritis Cartilage*, 11:65–77, 2003.

7. R. C. Appleyard, M. V. Swain, S. Khanna, and G. A. Murrell. The accuracy and reliability of a novel handheld dynamic indentation probe for analysing articular cartilage. *Phys Med Biol*, 46(2):541–550., 2001.

8. C. G. Armstrong and V. C. Mow. Variations in the intrinsic mechanical properties of human articular cartilage with age, degeneration, and water content. *J Bone Joint Surg Am*, 64(1):88–94, 1982.

9. J. P. Arokoski, M. M. Hyttinen, H. J. Helminen, and J. S. Jurvelin. Biomechanical and structural characteristics of canine femoral and tibial cartilage. *J Biomed Mater Res*, 48(2):99–107, 1999.

10. J. P. Arokoski, M. M. Hyttinen, T. Lapveteläinen, P. Takacs, B. Kosztaczky, L. Modis, V. Kovanen, and H. Helminen. Decreased birefringence of the superficial zone collagen network in the canine knee (stifle) articular cartilage after long distance running training, detected by quantitative polarised light microscopy. *Ann Rheum Dis*, 55(4):253–264, 1996.

11. J. P. Arokoski, J. S. Jurvelin, U. Väätäinen, and H. J. Helminen. Normal and pathological adaptations of articular cartilage to joint loading. *Scand J Med Sci Sports*, 10(4):186–198, 2000.

12. G. A. Ateshian, L. J. Soslowsky, and V. C. Mow. Quantitation of articular surface topography and cartilage thickness in knee joints using stereophotogrammetry. *J Biomech*, 24(8):761–776, 1991.

13. K. A. Athanasiou, A. Agarwal, A. Muffoletto, F. J. Dzida, G. Constantinides, and M. Clem. Biomechanical properties of hip cartilage in experimental animal models. *Clin Orthop*, (316):254–266, 1995.

14. K. A. Athanasiou, G. Constantinides, and D. R. Lanctot. Articular cartilage evaluator and method for using the same. *United States Patent*, page 5673 5708, 1995.

15. A. Benninghoff. Form und bau der gelenkknorpel in ihren beziehungen zur funktion. erste mitteilung: die modellierenden und formerhaltenden faktoren des knorpelreliefs. *Z Anat*, 76:43–63, 1925.

16. S. I. Berkenblit, E. H. Frank, E. P. Salant, and A. J. Grodzinsky. Nondestructive detection of cartilage degeneration using electromechanical surface spectroscopy. *J Biomech Eng*, 116(4):384–392, 1994.

17. G.P. Berry, J.C. Bamber, N.R. Miller, C.G. Armstrong, and P.E. Barbone. Towards an acoustic model-based poroelastic imaging method: I. theoretical foundation. *Ultrasound Med Biol*, 32(4):547–567, 2006.

18. G.P. Berry, J.C. Bamber, N.R. Miller, P.E. Barbone, N.L. Bush, and C.G. Armstrong. Towards an acoustic model-based poroelastic imaging method: II. experimental investigation. *Ultrasound Med Biol*, 32(12):1869–1885, 2006.

19. F.J. Blanco, R. Guitian, E. Vaguez-Martul, F.J. de Toro, and F. Galdo. Osteoarthritis chondrocytes die by apoptosis. *Arthritis rheum*, 41(2):284–289, 1998.

20. N. Blumenkrantz and G. Asboe-Hansen. New method for quantitative determination of uronic acids. *Anal Biochem*, 54(2):484–489, 1973.

21. P.L. Briant, J.H. Rylander, S.L. Bevill, and T.P. Andriacchi. Effects of altered loading on collagen matrix deformation in articular cartilage. *Trans Orthop Res Soc*, 32:607, 2007.

22. H. Brommer, M. S. Laasanen, P.A.J. Brama, P.R. van Weeren, A. Barneveld, H. J. Helminen, and J. S. Jurvelin. Influence of age, site and degenerative state on the speed of sound in equine articular cartilage. *Am J Vet Res*, 66:1175–1180, 2005.

23. N. D. Broom and C. A. Poole. Articular cartilage collagen and proteoglycans. their functional interdependency. *Arthritis Rheum*, 26(9):1111–1119, 1983.

24. A. E. Brown. *Rationale and summary of methods for determining ultrasonic properties of materials at Lawrence Livermore National Laboratory.* National Technical Information Service, U.S. Department of Commerce, Springfield, 1997.

25. J. A. Buckwalter and J. Martin. Degenerative joint disease. *Clin Symp*, 47(2):1–32, 1995.

26. J.A. Buckwalter and H.J. Mankin. Articular cartilage, part I: Tissue design and chonrocyte-matrix interactions. *J Bone Joint Surg Am*, 79(4):600–611, 1997.

27. J.A. Buckwalter and H.J. Mankin. Articular cartilage, part II: Degeneration and osteoarthritis, repair, regeneration, and transplantation. *J Bone Joint Surg Am*, 79(4):612–632, 1997.

28. I. Cespedes, J. Ophir, H. Ponnekanti, and N. Maklad. Elastography: elasticity imaging using ultrasound with application to muscle and breast in vivo. *Ultrason Imaging*, 15(2):73–88, 1993.

29. R. E. Challis and R. I. Kitney. Biomedical signal processing (in four parts). part 1. time-domain methods. *Med Biol Eng Comput*, 28(6):509–524, 1990.

30. E. H. Chiang, R. S. Adler, C. R. Meyer, J. M. Rubin, D. K. Dedrick, and T. J. Laing. Quantitative assessment of surface roughness using backscattered ultrasound: the effects of finite surface curvature. *Ultrasound Med Biol*, 20(2):123–135, 1994.

31. E. H. Chiang, T. J. Laing, C. R. Meyer, J. L. Boes, J. M. Rubin, and R. S. Adler. Ultrasonic characterization of in vitro osteoarthritic articular cartilage with validation by confocal microscopy. *Ultrasound Med Biol*, 23(2):205–213, 1997.

32. E. Chérin, A. Saïed, P. Laugier, P. Netter, and G. Berger. Evaluation of acoustical parameter sensitivity to age-related and osteoarthritic changes in articular cartilage using 50-MHz ultrasound. *Ultrasound Med Biol*, 24(3):341–354, 1998.

33. E. Chérin, A. Saïed, B. Pellaumail, D. Loeuille, P. Laugier, P. Gillet, P. Netter, and G. Berger. Assessment of rat articular cartilage maturation using 50-Mhz quantitative ultrasonography. *Osteoarthritis Cartilage*, 9:178–186, 2001.

34. B. Cohen, W. M. Lai, and V. C. Mow. A transversely isotropic biphasic model for unconfined compression of growth plate and chondroepiphysis. *J Biomech Eng*, 120(4):491–496, 1998.

35. E. Collett. *Polarized Light: Fundamentals and Applications*. Marcel Dekker Inc., New York, 1993.

36. J. H. Dashefsky. Arthroscopic measurement of chondromalacia of patella cartilage using a microminiature pressure transducer. *Arthroscopy*, 3(2):80–85, 1987.

37. D. G. Disler, E. Raymond, D. A. May, J. S. Wayne, and T. R. McCauley. Articular cartilage defects: in vitro evaluation of accuracy and interobserver reliability for detection and grading with US. *Radiology*, 215(3):846–851, 2000.

38. F. Eckstein, D. Burstein, and T.M. Link. Quantitative MRI of cartilage and bone: degenerative changes in osteoarthritis. *NMR Biomed.*, 19:822–854, 2006.

39. F. Eckstein, H. Sittek, S. Milz, E. Schulte, B. Kiefer, M. Reiser, and R. Putz. The potential of magnetic resonance imaging (MRI) for quantifying articular cartilage thickness - a methodological study. *Clin Biomech*, 10(8):434–440, 1995.

40. E. B. Evans, G. W. N. Eggers, J. K. Butler, and J. Blumel. Experimental immobilization and remobilization of rat knee joints. *J Bone Joint Surg Am*, 42-A(5):737–758, 1960.

41. E.C. Everbach. *Tissue composition determination via measurement of the acoustic nonlinearity parameter*. Yale University, New Haven, 1989.

42. H. Forster and Fisher J. The influence of loading time and lubricant on the friction of articular cartilage. *Proc Inst Mech Eng*, page 162, 1996.

43. M. Fortin, M. D. Buschmann, M. J. Bertrand, F. S. Foster, and J. Ophir. Dynamic measurement of internal solid displacement in articular cartilage using ultrasound backscatter. *J Biomech*, 36(3):443–447, 2003.

44. E. H. Frank and A. J. Grodzinsky. Cartilage electromechanics-I. Electrokinetic transduction and the effects of electrolyte pH and ionic strength. *J Biomech*, 20(6):615–627, 1987.

45. M. A. Freeman. Is collagen fatigue failure a cause of osteoarthrosis and prosthetic component migration? A hypothesis. *J Orthop Res*, 17(1):3–8, 1999.

46. M. I. Froimson, A. Ratcliffe, T. R. Gardner, and V. C. Mow. Differences in patellofemoral joint cartilage material properties and their significance to the etiology of cartilage surface fibrillation. *Osteoarthritis Cartilage*, 5(6):377–386, 1997.

47. G. E. Gold, D. Burstein, B. Dardzinski, P. Lang, F. Boada, and T. Mosher. MRI of articular cartilage in OA: novel pulse sequences and compositional/functional markers. *Osteoarthritis Cartilage*, 14 Suppl 1:76–86, 2006.

48. S. A. Goss and Jr. O'Brien, W. D. Direct ultrasonic velocity measurement of mammalian collagen threads. *J Acoust Soc Am*, 85:507–511, 1979.

49. S. A. Goss and Jr. O'Brien, W. D. Dependence of the ultrasonic properties of biological tissue of constituent proteins. *J Acoust Soc Am*, 67(3):1041–1044, 1980.

50. Jr. Harris, E. D., H. G. Parker, E. L. Radin, and S. M. Krane. Effects of proteolytic enzymes on structural and mechanical properties of cartilage. *Arthritis Rheum*, 15(5):497–503, 1972.

51. E. M. Hasler, W. Herzog, J. Z. Wu, W. Muller, and U. Wyss. Articular cartilage biomechanics: theoretical models, material properties, and biosynthetic response. *Crit Rev Biomed Eng*, 27(6):415–488, 1999.

52. K. Hattori, Y. Takakura, M. Ishimura, T. Habata, K. Uematsu, N. Tomita, and K. Ikeuch. Quantitative arthroscopic ultrasound evaluation of living human cartilage. *Clin Biomech*, 19:213–216, 2004.

53. W. C. Hayes, L. M. Keer, G. Herrmann, and L. F. Mockros. A mathematical analysis for indentation tests of articular cartilage. *J Biomech*, 5(5):541–551, 1972.

54. J. M. Herrmann, C. Pitris, B. E. Bouma, S. A. Boppart, C. A. Jesser, D. L. Stamper, J. G. Fujimoto, and M. E. Brezinski. High resolution imaging of normal and osteoarthritic cartilage with optical coherence tomography. *J Rheumatol*, 26(3):627–635, 1999.

55. R. Y. Hori and L. F. Mockros. Indentation tests of human articular cartilage. *J Biomech*, 9(4):259–268, 1976.

56. A. Hulth. Does osteoarthrosis depend on growth of the mineralized layer of cartilage? *Clin Orthop*, (287):19–24, 1993.

57. G. A. Joiner, E. R. Bogoch, K. P. Pritzker, M. D. Buschmann, A. Chevrier, and F. S. Foster. High frequency acoustic parameters of human and bovine articular cartilage following experimentally-induced matrix degradation. *Ultrason Imaging*, 23(2):106–116, 2001.

58. G. A. Joiner, E. R. Bogoch, K. P. Pritzker, M. D. Buschmann, and F. S. Foster. Changes in acoustic parameters at 30 Mhz of human and bovine cartilage following experimentally-induced matrix degradation to simulate early osteoarthritis. *IEEE Ultrasonics Symposium*, 2:1337–1340, 2000.

59. D. Joseph, W. Y. Gu, X. G. mao, W. M. Lai, and V. C. Mow. True density of normal and enzymatically treated bovine articular cartilage. *Trans. Orthop. Res. Soc.*, 24:642, 1-4.2.1999 1999.

60. P. Julkunen, P. Kiviranta, W. Wilson, J. S. Jurvelin, and R. K. Korhonen. Characterization of articular cartilage by combining microscopic analysis with a fibril-reinforced finite element model. *J Biomech*, (in press, doi:10.1016/j.jbiomech.2006.07.026), 2007.

61. J. S. Jurvelin, M. D. Buschmann, and E. B. Hunziker. Optical and mechanical determination of Poisson's ratio of adult bovine humeral articular cartilage. *J Biomech*, 30(3):235–241, 1997.

62. J. S. Jurvelin, M. D. Buschmann, and E. B. Hunziker. Mechanical anisotropy of the human knee articular cartilage in compression. *Proc Inst Mech Eng*, 217:215–219, 2003.

63. J. S. Jurvelin, T. Räsänen, P. Kolmonen, and T. Lyyra. Comparison of optical, needle probe and ultrasonic techniques for the measurement of articular cartilage thickness. *J Biomech*, 28(2):231–235, 1995.

64. E. Kaleva, S. Saarakkala, J. Töyräs, H. J. Nieminen, and J. S. Jurvelin. Comparison of time domain, frequency domain and wavelet ultrasound analysis for diagnosing cartilage degeneration. *Trans Orthop Res Soc*, 32:705, 2007.

65. G. N. Kawchuk and P. D. Elliott. Validation of displacement measurements obtained from ultrasonic images during indentation testing. *Ultrasound Med Biol*, 24(1):105–111, 1998.

66. M. J. Kääb, K. Ito, J. M. Clark, and H. P. Notzli. Deformation of articular cartilage collagen structure under static and cyclic loading. *J Orthop Res*, 16(6):743–751, 1998.

67. M. J. Kääb, K. Ito, B. Rahn, J. M. Clark, and H. P. Notzli. Effect of mechanical load on articular cartilage collagen structure: A scanning electron-microscopic study. *Cells Tissues Organs*, 167:106–120, 2000.

68. G. E. Kempson, M. A. Freeman, and S. A. Swanson. The determination of a creep modulus for articular cartilage from indentation tests of the human femoral head. *J Biomech*, 4(4):239–250, 1971.

69. H. K. Kim, P. S. Babyn, K. A. Harasiewicz, H. K. Gahunia, K. P. Pritzker, and F. S. Foster. Imaging of immature articular cartilage using ultrasound backscatter microscopy at 50 MHz. *J Orthop Res*, 13(6):963–970, 1995.

70. L.E. Kinsler and A.R. Frey. *Fundamentals of acoustics*. John Wiley & Sons, Inc., New York, 1950.

71. K. Király, M. M. Hyttinen, T. Lapveteläinen, M. Elo, I. Kiviranta, J. Dobai, L. Modis, H. J. Helminen, and J. P. Arokoski. Specimen preparation and quantification of collagen birefringence in unstained sections of articular cartilage using image analysis and polarizing light microscopy. *Histochem J*, 29(4):317–327, 1997.

72. K. Király, M. Lammi, J. Arokoski, T. Lapveteläinen, M. Tammi, H. Helminen, and I. Kiviranta. Safranin O reduces loss of glycosaminoglycans from bovine articular cartilage during histological specimen preparation. *Histochem J*, 28(2):99–107, 1996.

73. K. Király, T. Lapveteläinen, J. Arokoski, K. Törrönen, L. Modis, I. Kiviranta, and H. J. Helminen. Application of selected cationic dyes for the semiquantitative estimation of glycosaminoglycans in histological sections of articular cartilage by microspectrophotometry. *Histochem J*, 28(8):577–590, 1996.

74. I. Kiviranta, J. Rieppo, R. K. Korhonen, P. Julkunen, J. Töyräs, and J.S. Jurvelin. Collagen network primarily controls Poisson's ratio of bovine articular cartilage in compression. *J Orthop Res*, 24(4):690–699, 2006.

75. I. Kiviranta, M. Tammi, J. Jurvelin, J. Arokoski, A. M. Säämänen, and H. J. Helminen. Articular cartilage thickness and glycosaminoglycan distribution in the young canine knee joint after remobilization of the immobilized limb. *J Orthop Res*, 12(2):161–167, 1994.

76. P. Kolmonen, T. Lyyra, and J.S. Jurvelin. Experimental comparison of acoustic and mechanical properties of bovine knee articular cartilage. *Trans Orthop Res Soc*, 19:513, 1995.

77. E. E. Konofagou, T. P. Harrigan, J. Ophir, and T. A. Krouskop. Poroelastography: imaging the poroelastic properties of tissues. *Ultrasound Med Biol*, 27(10):1387–1397, 2001.

78. R. K. Korhonen, M. S. Laasanen, J. Töyräs, R. Lappalainen, H. J. Helminen, and J. S. Jurvelin. Fibril reinforced poroelastic model predicts specifically mechanical behavior of normal, proteoglycan depleted and collagen degraded articular cartilage. *J Biomech*, 36(9):1373–1379, 2003.

79. R. K. Korhonen, S. Saarakkala, J. Töyräs, M. S. Laasanen, I. Kiviranta, and J. S. Jurvelin. Experimental and numerical validation for the novel configuration of an arthroscopic indentation instrument. *Phys Med Biol*, 48(11):1565–1576, 2003.

80. M. S. Laasanen, J. Töyräs, J. Hirvonen, S. Saarakkala, R. K. Korhonen, M. T. Nieminen, I. Kiviranta, and J. S. Jurvelin. Novel mechano-acoustic technique and instrument for diagnosis of cartilage degeneration. *Physiol Meas*, 23:491–503, 2002.

81. M. S. Laasanen, J. Töyräs, J. Hirvonen, S. Saarakkala, R. K. Korhonen, M. T. Nieminen, I. Kiviranta, and J. S. Jurvelin. Ultrasound indentation of bovine knee articular cartilage in situ. *J Biomech*, 36:1259–1267, 2003.

82. M. S. Laasanen, J. Töyräs, R. K. Korhonen, J. Rieppo, S. Saarakkala, M. T. Nieminen, J. Hirvonen, and J. S. Jurvelin. Biomechanical properties of knee articular cartilage. *Biorheology*, 40(1-3):133–140, 2003.

83. M. S. Laasanen, J. Töyräs, A. Vasara, M. M. Hyttinen, S. Saarakkala, J. Hirvonen, J. S. Jurvelin, and I. Kiviranta. Mechano-acoustic diagnosis of cartilage degeneration and repair. *J Bone Joint Surg Am*, 85-A:78–84, 2003.

84. M.S. Laasanen, S. Saarakkala, J. Töyräs, J. Rieppo, and J.S. Jurvelin. Site-specific ultrasound reflection properties and superficial collagen content of bovine knee articular cartilage. *Phys Med Biol*, 50:3221–3233, 2005.

85. M.S. Laasanen, J. Töyräs, A. Vasara, S. Saarakkala, M.M. Hyttinen, I. Kiviranta, and Jurvelin J.S. Quantitative ultrasound imaging of spontaneous repair of porcine cartilage. *Osteoarthritis Cartilage*, 14(3):258–263, 2006.

86. W. M. Lai, J. S. Hou, and V. C. Mow. A triphasic theory for the swelling and deformation behaviors of articular cartilage. *J Biomech Eng*, 113(3):245–258, 1991.

87. C. M. Langton, S. B. Palmer, and R. W. Porter. The measurement of broadband ultrasonic attenuation in cancellous bone. *Eng Med*, 13(2):89–91, 1984.

88. S. Lees, J.D. Heeley, J.M. Ahern, and M.G. Oravecz. Axial phase velocity in rat tail tendon fibers at 100 MHz by ultrasonic microscopy. *IEEE Trans Sonics Ultrason*, 30(2):85–90, 1983.

89. F. Lefebvre, N. Graillat, E. Chérin, G. Berger, and A. Saïed. Automatic three-dimensional reconstruction and characterization of articular cartilage from high-resolution ultrasound acquisitions. *Ultrasound Med Biol*, 24(9):1369–1381, 1998.

90. J. Leidy. On the intimate structure and history of the articular cartilages. *Am J Med Sci*, 34:277–295, 1849.

91. L. P. Li, M. D. Buschmann, and A. Shirazi-Adl. Alterations in mechanical behaviour of articular cartilage due to changes in depth varying material properties - a nonhomogeneous poroelastic model study. *Comput Methods Biomech Biomed Engin*, 5(1):45–52, 2002.

92. M.H. Lu, Y. P. Zheng, and Q.H. Huang. A novel noncontact ultrasound indentation system for measurement of tissue material properties using water jet compression. *Ultrasound Med Biol*, 31(6):817–826, 2005.

93. X.L. Lu, C. Miller, X. E. Guo, and V. C. Mow. Triphasic indentation of articular cartilage: determination of both mechanical properties and fixed charge density. *Trans Orthop Res Soc*, 31:294, 2006.

94. T. Lyyra, J. Jurvelin, P. Pitkänen, U. Väätäinen, and I. Kiviranta. Indentation instrument for the measurement of cartilage stiffness under arthroscopic control. *Med Eng Phys*, 17(5):395–399, 1995.

95. A. F. Mak. Unconfined compression of hydrated viscoelastic tissues: a biphasic poroviscoelastic analysis. *Biorheology*, 23(4):371–383, 1986.

96. H. J. Mankin, H. Dorfman, L. Lippiello, and A. Zarins. Biochemical and metabolic abnormalities in articular cartilage from osteo-arthritic human hips. II. Correlation of morphology with biochemical and metabolic data. *J Bone Joint Surg Am*, 53(3):523–537, 1971.

97. A. Maroudas and M. Venn. Chemical composition and swelling of normal and osteoarthrotic femoral head cartilage. II. swelling. *Ann Rheum Dis*, 36(5):399–406., 1977.

98. V. E. Modest, M. C. Murphy, and R. W. Mann. Optical verification of a technique for in situ ultrasonic measurement of articular cartilage thickness. *J Biomech*, 22(2):171–176, 1989.

99. L. Modis. *Organization of the extracellular matrix: a polarization microscopic approach*. CRC Press, Boca Raton, 1991.

100. V. C. Mow, M. C. Gibbs, W. M. Lai, W. B. Zhu, and K. A. Athanasiou. Biphasic indentation of articular cartilage II. A numerical algorithm and an experimental study. *J Biomech*, 22(8-9):853–861, 1989.

101. V. C. Mow, A. Ratcliffe, and A. R. Poole. Cartilage and diarthrodial joints as paradigms for hierarchical materials and structures. *Biomaterials*, 13(2):67–97, 1992.

102. V. C. Mow, W. Zhu, and A. Ratcliffe. Structure and function of articular cartilage and meniscus. In V. C. Mow and W. C. Hayes, editors, *Basic orthopaedic biomechanics*, pages 143–198. Raven Press, Ltd, New York, 1991.

103. S. Myers, K. Dines, M. Albrecht, D. Brandt, E. Wu, and K. Brandt. Assessment by high frequency ultrasound (HFU) of the thickness and subsurface characteristics of normal and osteoarthritic human cartilage. *Trans Orthop Res Soc*, 18:215, 1994.

104. S. L. Myers, K. Dines, D. A. Brandt, K. D. Brandt, and M. E. Albrecht. Experimental assessment by high frequency ultrasound of articular cartilage thickness and osteoarthritic changes. *J Rheumatol*, 22(1):109–116, 1995.

105. M. Q. Niederauer, S. Cristante, G. M. Niederauer, R. P. Wilkes, S. M. Singh, D. F. Messina, M. A. Walter, B. D. Boyan, J. C. DeLee, and G. Niederauer. A novel instrument for quantitatively measuring the stiffness of articular cartilage. *Trans Orthop Res Soc*, 23:905, 1998.

106. M. Nissi, J. Töyräs, M. S. Laasanen, J. Rieppo, S. Saarakkala, R. Lappalainen, J. S. Jurvelin, and M. T. Nieminen. Proteoglycan and collagen sensitive MRI evaluation of normal and degenerated articular cartilage. *J Orthop Res*, 22(3):557–564, 2004.

107. H. Nötzli, A. Wilson, F. Forster, and J. Clark. Automated ultrasound measurements can map contour and thickness of articular cartilage. *Trans Orthop Res Soc*, 18:409, 1994.

108. J. Ophir, S. K. Alam, B. Garra, F. Kallel, E. Konofagou, T. Krouskop, and T. Varghese. Elastography: ultrasonic estimation and imaging of the elastic properties of tissues. *Proc Inst Mech Eng [H]*, 213(3):203–233, 1999.

109. J. Ophir, I. Cespedes, H. Ponnekanti, Y. Yazdi, and X. Li. Elastography: a quantitative method for imaging the elasticity of biological tissues. *Ultrason Imaging*, 13(2):111–134, 1991.

110. J. Ophir and P. Jaeger. Spectral shifts of ultrasonic propagation through media with nonlinear dispersive attenuation. *Ultrason Imaging*, 4(3):282–289, 1982.

111. J. Ophir and Y. Yazdi. A transaxial compression technique (TACT) for localized pulse-echo estimation of sound speed in biological tissues. *Ultrason Imaging*, 12:35–46, 1990.

112. J. R. Parsons and J. Black. The viscoelastic shear behavior of normal rabbit articular cartilage. *J Biomech*, 10(1):21–29, 1977.

113. S.G. Patil, Y.P. Zheng, J.Y. Wu, and J. Shi. Measurement of depth-dependence and anisotropy of ultrasound speed of bovine articular cartilage in vitro. *Ultrasound Med Biol*, 30:953–961, 2004.

114. B. Pellaumail, V. Dewailly, A. Watrin, D. Loeuille, P. Netter, G. Berger, and A. Saïed. Attenuation coefficient and speed of sound in immature and mature rat cartilage: a study in the 30-70 MHz frequency range. *IEEE Ultrasonics Symposium*, pages 1361–1365, 1999.

115. B. Pellaumail, A. Watrin, D. Loeuille, P. Netter, G. Berger, P. Laugier, and A. Saied. Effect of articular cartilage proteoglycan depletion on high frequency ultrasound backscatter. *Osteoarthritis Cartilage*, 10(7):535–541, 2002.

116. J. Pohlhammer and Jr. O'Brien, W. D. Dependence of the ultrasonic scatter coefficient on collagen concentration in mammalian tissues. *J Acoust Soc Am*, 69(1):283–285, 1981.

117. L. Qin, Y. Zheng, C. Leung, A. Mak, W. Choy, and K. Chan. Ultrasound detection of trypsin-treated articular cartilage: its association with cartilaginous proteoglycans assessed by histological and biochemical methods. *J Bone Miner Metab*, 20(5):281–287, 2002.

118. E. L. Radin and R. M. Rose. Role of subchondral bone in the initiation and progression of cartilage damage. *Clin Orthop*, (213):34–40, 1986.

119. J. Rieppo, J. Hallikainen, J. S. Jurvelin, H. J. Helminen, and M. M. Hyttinen. Novel quantitative polarization microscopic assessment of cartilage and bone collagen birefringence, orientation and anisotropy. *Trans Orthop Res Soc*, 28:570, 2003.

120. J. Rieppo, M. M. Hyttinen, R. Lappalainen, J. S. Jurvelin, and H. J. Helminen. Spatial determination of water, collagen and proteoglycan contents by Fourier transform infrared imaging and digital densitometry. *Trans Orthop Res Soc*, 28:1021, 2004.

121. J. Rieppo, P. Julkunen, H. J. Helminen, and J. S. Jurvelin. Changes in composition of articular cartilage under static loading conditions: quantitative analysis with FT-IRIS and FE model. *Trans Orthop Res Soc*, 32:626, 2007.

122. J. Rieppo, J. Töyräs, M. T. Nieminen, V. Kovanen, M. M. Hyttinen, R. Korhonen, J. S. Jurvelin, and H. J. Helminen. Structure-function relationships in enzymatically modified articular cartilage. *Cells Tissues Organs*, 175:121–132, 2003.

123. J.L. Rose and B.B. Goldberg. *Basic physics in diagnostic ultrasound*. John Wiley & Sons, New York, 1979.

124. J. Rothfuss, W. Mau, H. Zeidler, and M.H. Brenner. Socioeconomic evaluation of rheumatoid arthritis and osteoarthritis: a literature review. *Semin Arthritis Rheum*, 26(5):771–779, 1997.

125. P. D. Rushfeldt, R. W. Mann, and W. H. Harris. Improved techniques for measuring in vitro the geometry and pressure distribution in the human acetabulum-I. Ultrasonic measurement of acetabular surfaces, sphericity and cartilage thickness. *J Biomech*, 14(4):253–260, 1981.

126. S. Saarakkala. *Pre-clinical ultrasound diagnostics of articular cartilage and subchondral bone*. University of Kuopio, Kuopio, Finland, 2007.

127. S. Saarakkala, M.S. Laasanen, J.S. Jurvelin, and J. Töyräs. Quantitative ultrasound imaging detects degenerative changes in articular cartilage surface and subchondral bone. *Phys Med Biol*, 20(20):5333–5346, 2006.

128. S. Saarakkala, J. Töyräs, J. Hirvonen, M.S. Laasanen, R. Lappalainen, and J.S. Jurvelin. Ultrasonic quantitation of superficial degradation of articular cartilage. *Ultrasound Med Biol*, 30(6):783–792, 2004.

129. J. R. Sachs and A. J. Grodzinsky. Electromechanical spectroscopy of cartilage using a surface probe with applied mechanical displacement. *J Biomech*, 28(8):963–976, 1995.

130. A. Saïed, E. Chérin, H. Gaucher, P. Laugier, P. Gillet, J. Floquet, P. Netter, and G. Berger. Assessment of articular cartilage and subchondral bone: subtle and progressive changes in experimental osteoarthritis using 50 MHz echography in vitro. *J Bone Miner Res*, 12(9):1378–1386, 1997.

131. H. Sandmark. *Knee osteoarthrosis in relation to physical workload and lifestyle factors - epidemiological studies*. National Institute for Working Life, Stockholm, 1999.

132. D. E. Schwartz, Y. Choi, L. J. Sandell, and W. R. Hanson. Quantitative analysis of collagen, protein and DNA in fixed, paraffin-embedded and sectioned tissue. *Histochem J*, 17(6):655–663, 1985.

133. C.M. Sehgal. Quantitative relationship between tissue composition and scattering of ultrasound. *J Acoust Soc Am*, 94(4):1944–1952, 1993.

134. D. A. Senzig, F. K. Forster, and J. E. Olerud. Ultrasonic attenuation in articular cartilage. *J Acoust Soc Am*, 92(2 Pt 1):676–681, 1992.

135. D.E.T. Shepherd and B.B. Seedhom. A technique for measuring the compressive modulus of articular cartilage under physiological loading rates with preliminary results. *Proc Inst Mech Eng*, 211:155–165, 1997.

136. W. D. Shingleton, D. J. Hodges, P. Brick, and T. E. Cawston. Collagenase: a key enzyme in collagen turnover. *Biochem Cell Biol*, 74(6):759–775, 1996.

137. P.J. Shull, editor. *Nondestructive evaluation: theory, techniques and applications*. Marcel Dekker Inc., New York, 2002.

138. M. P. Spriet, C. A. Girard, S. F. Foster, K. Harasiewicz, D. W. Holdsworth, and S. Laverty. Validation of a 40MHz B-scan ultrasound biomicroscope for the evaluation of osteoarthritis lesions in an animal model. *Osteoarthritis Cartilage*, 13:171–179, 2005.

139. J. K. Suh, I. Youn, and F. H. Fu. An in situ calibration of an ultrasound transducer: a potential application for an ultrasonic indentation test of articular cartilage. *J Biomech*, 34(10):1347–1353, 2001.

140. P. A. Torzilli. Mechanical response of articular cartilage to an oscillating load. *Mech Res Comm*, 11:75–82, 1984.

141. J.G. Truscott and R. Strelitzki. Challenges in the ultrasonic measurement of bone. In F.A. Duck, A.C. Baker, and H.C. Starritt, editors, *Ultrasound in medicine*, Medical Science Series, pages 287–306. Institute of Physics Publishing, London, 1998.

142. J. Töyräs, M. S. Laasanen, S. Saarakkala, M. Lammi, J. Rieppo, J. Kurkijärvi, R. Lappalainen, and J. S. Jurvelin. Speed of sound in normal and degenerated bovine articular cartilage. *Ultrasound Med Biol*, 29:447–454, 2003.

143. J. Töyräs, T. Lyyra-Laitinen, M. Niinimäki, R. Lindgren, M. T. Nieminen, I. Kiviranta, and J. S. Jurvelin. Estimation of the Young's modulus of articular cartilage using an arthroscopic indentation instrument and ultrasonic measurement of tissue thickness. *J Biomech*, 34(2):251–256, 2001.

144. J. Töyräs, H. J. Nieminen, M. S. Laasanen, M. T. Nieminen, R. K. Korhonen, J. Rieppo, J. Hirvonen, H. J. Helminen, and J. S. Jurvelin. Ultrasonic characterization of articular cartilage. *Biorheology*, 39:161–169, 2002.

145. J. Töyräs, J. Rieppo, M. T. Nieminen, H. J. Helminen, and J. S. Jurvelin. Characterization of enzymatically induced degradation of articular cartilage using high frequency ultrasound. *Phys Med Biol*, 44(11):2723–2733, 1999.

146. P. N. T. Wells. *Physical Principles of Ultrasonic Diagnosis*. Academic Press, London, 1969.

147. P. N. T. Wells. Review: absorption and dispersion of ultrasound in biological tissue. *Ultrasound Med Biol*, 1(4):369–376, 1975.

148. P. N. T. Wells. *Biomedical ultrasonics*. Academic Press, London, 1977.

149. W. Wilson, J. M. Huyghe, and C. C. van Donkelaar. A composition-based cartilage model for the assessment of compositional changes during cartilage damage and adaptation. *Osteoarthritis Cartilage*, 14(6):554–560, 2006.

150. W. Wilson, C. C. van Donkelaar, B. van Rietbergen, K. Ito, and R. Huiskes. Stresses in the local collagen network of articular cartilage: a poroviscoelastic fibril-reinforced element study. *J Biomech*, 37:357–366, 2004.

151. W. Wilson, C. C. van Donkelaar, B. van Rietbergen, K. Ito, and R. Huiskes. Erratum to "Stresses in the local collagen network of articular cartilage: a poroviscoelastic fibril-reinforced finite element study" [Journal of Biomechanics 37 (2004) 357-366] and "A fibril-reinforced poroviscoelastic swelling model for articular cartilage" [Journal of Biomechanics 38 (2005) 1195-1204]. *J Biomech*, 38(10):2138–2140, 2005.

152. W. Wilson, B. van Rietbergen, C. C. van Donkelaar, and R. Huiskes. Pathways of load-induced cartilage damage causing cartilage degeneration in the knee after meniscectomy. *J Biomech*, 36(6):845–851, 2003.

153. J. Q. Yao and B. B. Seedhom. Ultrasonic measurement of the thickness of human articular cartilage in situ. *Rheumatology (Oxford)*, 38(12):1269–1271, 1999.

154. E. Yelin and L. F. Callahan. The economic cost and social and psychological impact of musculoskeletal conditions. National Arthritis Data Work Groups. *Arthritis Rheum*, 38(10):1351–1362, 1995.

155. I. Youn, F.H. Fu, and J-K. Suh. Determination of the mechanical properties of articular cartilage using a high-frequency ultrasonic indentation technique. *Trans Orthop Res Soc*, 23:162, 1999.

156. Y. P. Zheng, C. X. Ding, J. Bai, A. F. Mak, and L. Qin. Measurement of the layered compressive properties of trypsin-treated articular cartilage: an ultrasound investigation. *Med Biol Eng Comput*, 39(5):534–541, 2001.

157. Y. P. Zheng and A. F. Mak. An ultrasound indentation system for biomechanical properties assessment of soft tissues in-vivo. *IEEE Trans Biomed Eng*, 43(9):912–918, 1996.

158. Y.P. Zheng, S.L. Bridal, J. Shi, A. Saied, M.H. Lu, B. Jaffre, A.F.T. Mak, and P. Laugier. High resolution ultrasound elastomicroscopy imaging of soft tissues: system development and feasibility. *Phys Med Biol*, 49:3925–3938, 2004.

159. Y.P. Zheng, A.F.T. Mak, K.P. Lau, and L. Qin. An ultrasonic measurement for in vitro depth-dependent equilibrium strains of articular cartilage in compression. *Phys Med Biol*, 47:3165–3180, 2002.

160. Y.P. Zheng, H.J. Niu, A.F.T. Mak, and Y.P. Huang. Ultrasonic measurement of depth-dependent transient behaviors of articular cartilage under compression. *J Biomech*, 39(9):1830–1837, 2005.

Kuopio University Publications C. Natural and Environmental Sciences

C 196. Heijari, Juha. Seed origin, forest fertilization and chemical elicitor influencing wood characteristics and biotic resistance of Scots pine.
2006. 39 p. Acad. Diss.

C 197. Hakulinen, Mikko. Prediction of density, structure and mechanical properties of trabecular bone using ultrasound and X-ray techniques.
2006. 84 p. Acad. Diss.

C 198. Al Natsheh, Anas. Quantum Mechanics Study of Molecular Clusters Composed of Atmospheric Nucleation Precursors.
2006. 55 p. Acad. Diss.

C 199. Tarvainen, Tanja. Computational Methods for Light Transport in Optical Tomography.
2006. 123 p. Acad. Diss.

C 200. Heikkinen, Päivi. Studies on Cancer-related Effects of Radiofrequency Electromagnetic Fields. 2006. 165 p. Acad. Diss.

C 201. Laatikainen, Tarja. Pesticide induced responses in ectomycorrhizal fungi and symbiont Scots pine seedlings.
2006. 180 p. Acad. Diss.

C 202. Tiitta, Markku. Non-destructive methods for characterisation of wood material.
2006. 70 p. Acad. Diss.

C 203. Lehesranta, Satu. Proteomics in the Detection of Unintended Effects in Genetically Modified Crop Plants.
2006. 71 p. Acad. Diss.

C 204. Boman, Eeva. Radiotherapy forward and inverse problem applying Boltzmann transport equation.
2007. 138 p. Acad. Diss.

C 205. Saarakkala, Simo. Pre-Clinical Ultrasound Diagnostics of Articular Cartilage and Subchondral Bone.
2007. 96 p. Acad. Diss.

C 206. Korhonen, Samuli-Petrus. FLUFF-BALL, a Fuzzy Superposition and QSAR Technique - Towards an Automated Computational Detection of Biologically Active Compounds Using Multivariate Methods.
2007. 154 p. Acad. Diss.

C 207. Matilainen, Merja. Identification and characterization of target genes of the nuclear reseptors VDR and PPARs: implementing in silico methods into the analysis of nuclear receptor regulomes.
2007. 112 p. Acad. Diss.

C 208. Anttonen, Mikko J. Evaluation of Means to Increase the Content of Bioactive Phenolic Compounds in Soft Fruits.
2007. 93 p. Acad. Diss.

C 209. Pirkanniemi, Kari. Complexing agents: a study of short term toxicity, catalytic oxidative degradation and concentrations in industrial waste waters.
2007. 83 p. Acad. Diss.

C 210. Leppänen, Teemu. Effect of fiber orientation on cockling of paper.
2007. 96 p. Acad. Diss.